SELF-ASSMBLED LITHOGRAPHY-FREE FABRICATION OF MICROCHANNELS AND MICROFLUIDICS IN POLYMERS

by

WINTANA TADESSE KAHSAI

Presented to the Faculty of the Graduate School of
The University of Texas at Arlington in Partial Fulfillment
of the Requirements
for the Degree of

MASTER OF SCIENCE IN BIOMEDICAL ENGINEERING

THE UNIVERSITY OF TEXAS AT ARLINGTON
MAY 2012

ACKNOWLEDGEMENTS

First I would like to express my deepest gratitude to my advisor Dr. Samir Iqbal for giving me an opportunity to work in his lab and encouraging me to write this thesis. This opportunity made every second of my UT Arlington experience worthwhile. I feel amazingly fortunate to have an advisor who allowed me to express my ideas freely and creatively and at the same time guided me in times my steps were faltered. Working with him not only helped me progress academically but also progress as a person. With God, I hope I could pay it forward to uplift and inspire others.

Most importantly, I would like to thank my family who have been my rock throughout the years and dreamed bigger dreams for me than I could ever dream for myself. This would not have been possible without their love and patience. I cherish the encouragement and support they gave me throughout the years. In particular, I dedicate this thesis to my father, Tadesse Birhane, who is a strong advocate for education.

I would also like to thank all my friends and colleagues. I greatly value their friendship and deeply appreciate them for sharing their ideas and also keeping me sane through the hard time. Now I would like to take this opportunity to list my friends in alphabetical order who have contributed in this thesis: Adhanet Asgedom, Waseem Asghar, Dessalegn Atnafu, Swati Goyal, Rezene Haile, Hiwot Mekuria, Phenjun Offerle, Uyen Pham, Jeyantt Sankaran, Ahmed Shahid, Getu Tesso and Tewodros Wondimagegn. I also thank the staff of the Nanotechnology Research and Teaching Facility for their friendly service and support.

Above all I am grateful to God for blessing my life with people who are loving and inspiring.

March 28, 2012

ABSTRACT

SELF-ASSMBLED LITHOGRAPHY-FREE FABRICATION OF MICROCHANNELS AND MICROFLUIDICS IN POLYMERS

Wintana T. Kahsai, MS.

University of Texas at Arlington, 2012

Supervising Professor: Samir M. Iqbal

Rapid, reliable and easy to implement approaches are needed for fabrication of circular microchannels in polymeric microfluidics. PDMS has been a choice of material in microfluidics and it is being used as prototype due to its unique property such as flexibility and transparency. Traditional method of fabrication such as photolithography and soft lithography are complicated and time consuming. In this thesis, a non-lithography and bottom-up self-assembled approach is shown. The resulting devices can have uses in many applications such as assays, biosensing, separation of mixtures, micro-mixing and bioreactors.

This thesis presents novel approaches of manufacturing self-assembled microchannels in polydimethyleneoxide (PDMS) membranes. The underlying principle is based on the hydrophobic-hydrophilic interactions of different molecules with PDMS. Iron-oxide nanoparticles, acetone, and polymers such as polyurethane (PU) and poly (ethylene oxide) (PEO) are hydrophilic materials used to induce channel formation in the membranes of PDMS which is hydrophobic. The process is systematic, flexible in design, easy to implement, rapid, inexpensive and does not require lithography.

The technique yielded a controlled way to fabricate microchannels with a range of pore sizes, porosity and lengths. This was done by tweaking various parameters such as temperature, curing agent concentration, magnetic field, and different types of hydrophilic particles. Results showed channel diameters ranged from 500 nm - 900 μm. Fluid flow and

mixing of fluids in plasma treated microchannels under capillary action was also demonstrated and analyzed.

TABLE OF CONTENTS

LIST OF ILLUSTRATIONS

Figure Page

LIST OF TABLES

Table Page

CHAPTER 1
INTRODUCTION

Microfluidic devices provide a number of advantageous features for microscale systems. The volume of fluids needed in these devices is in micro and nanoliter ranges. Many biochemical reactions can be done on such small volumes of samples in controlled microenvironment of microfluidic systems.

To make microfluidic systems, polydimethylsiloxane (PDMS) is widely used. Molds for microfluidic channels are made by producing a master pattern in photoresist on the surface of the silicon wafer by photo- or e-beam lithography in most applications. These techniques are usually time consuming and expensive.

This thesis presents, develops and analyzes a technique of microchannels fabrication in PDMS which is carried out using bench-top tools, without the need of lithography or any specialized facilities or equipment. The fundamental principle is based on the self-assembly and directionality of microparticles through simple entropic and enthalpic interactions to construct well controlled microchannels in PDMS membrane. Our method reduces cost as well as avoids the complicated steps and materials involved in standard microchannel fabrication.

1.1 Objective

The aim of this thesis is to develop an efficient and rapid fabrication method of microchannels for applications such as microfluidics and bioreactors by simply using the surface property of particles.

1.2 Overview of Thesis

This thesis explores different techniques of fabrication for microchannels inside a PDMS membrane. The techniques are based on a simple bench top, self-assembled method using

hydrophobic and hydrophilic interactions of particles. This is done using PDMS as a base membrane which is hydrophobic. Different hydrophilic particles are explored and analyzed to fabricate various channel types. The next chapter explores literature review over current diagnostic devices, fabrication methods and their limitations. Fabrication concept and evidence of the proposed method is discussed in chapter 3. This chapter also shows results found using non polymeric hydrophilic materials such as iron-oxide nanoparticles and acetone. Chapter 4 covers channel formation using two different hydrophilic polymers, polyurethane and poly (ethylene oxide). The last chapter discusses some proposals that can be basis for future work.

1.3 Non-Polymeric Hydrophilic Particles

Various types of hydrophilic particles were used in the experiments. The non-polymeric hydrophilic particles were made of vaporized particles, acetone droplets and iron-oxide nanoparticles. Variations in curing agent and temperature were used to control pore size and porosity. Different ratio of acetone was used to fabricate ranges of pore sizes while a magnetic force was used to control the direction and alignment of iron-oxide nanoparticles. The general technique involved mixing of hydrophobic matrix with hydrophilic particles led to phase separation. During this process, hydrophilic particles were pushed to the top leaving hollow channels inside the PDMS membrane.

1.4 Polymer Hydrophilic Particles

Polymeric hydrophilic particle were also explored using a similar technique. Two types of polymers were explored: polyurethane (PU) and poly (ethylene oxide) (PEO). These were heated to form a viscous solution prior to mixing with PDMS. The change in entropy and enthalpy during PDMS polymerization and diffusion of low molar mass hydrophobic PDMS chains slowly pushed the molten polymer from bottom up. This movement resulted in the hollow voids in the form of empty channels in the PDMS bulk.

All the techniques mentioned above did not require any specialized equipment and only used hydrophobic-hydrophilic interactions of various microparticles incorporated with PDMS. We were able to fabricate channels with controlled depth, pore size, and porosity by using different type of hydrophilic particles and tweaking parameters such as temperature and curing agent. The membrane fabricated can have many applications such as in drug delivery, cell culture studies, separation of mixtures, and lap-on-a-chip technology. Fluid flow inside the microchannels was also analyzed. Fluid was transferred to the microchannels using capillary action and the velocity of fluid flow was analyzed. The system was also used as bioreactor to mix different solutions inside the microchannels.

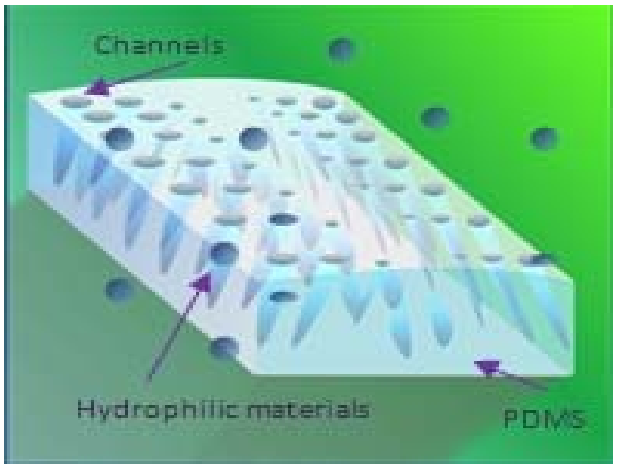

Figure 1.1 Schematic diagram of hydrophobic-hydrophilic interaction resulting in channel formation.

CHAPTER 2

LITRATURE REVIEW AND BACKGROUND

2.1 Microfluidics

Microfluidic devices have many applications in sensing, assaying, implants, etc. The amount of fluid in these applications is miniaturized to micro and nano ranges. Miniaturized devices offer many advantages over macroscale devices due to their high surface area to volume ratio. This contributes to their small requirements for solvents, reagents, reaction times, analysis of DNA chips, and lab-on-a-chip [10]. The reduced scale of the devices provides better manipulation of biological samples, since the dimension mimics those of a biological system [11-16]. The miniaturized devices are also favorable due to reduced cost for processing biological samples like DNA, enzymes, and media.

Microfluidic devices can allow precise control of the environment surrounding individual cells and the volume used in these experiments. Also, by using computer control system and running a number of assays in parallel, analysis time can be reduced. This way the results are more accurate and efficient. In addition to that, miniaturized samples have advantages in reduction of harmful chemicals. Thus waste products dumped are reduced to produce a safer environment.

Microfluidics is based on transport of bio/chemical samples at the micro-scale. The purpose of these devices is to reduce cost, work efficiently and rapidly. Currently, most systems use external macro elements attached to microdevices for transportation purpose. Some of the external processors used are pumps, temperature, and computers. While these techniques have advantages such as precision and high throughput, the systems are complex

and costly. To replace these macro processors to a microscale that can perform multiple tasks, efficient and inexpensive ways are still under investigation.

The three major ways of achieving fluid flow in microchannels are pressure-driven, electric-driven, and capillary action driven. High pressure difference is dependent on volumetric flow rate (Q). The flow rate is related to the pressure difference and the size of the channel by $Q=\Delta PR^4/\ 8\ \eta l$. ΔP is the pressure difference between the ends of the vessel, R is the radius of the vessel, l is length of the vessel, and η is the viscosity of the blood. The velocity of fluid on the other hand changes depending on the position across the channel. Even though pressure difference works well to control flow in a channel, the difference in velocity change which creates a parabolic type profile disperses samples. Pumps are also used to push or pull liquids as macro scale external elements attached to the micro devices. While the system in general is convenient in research facilities, it defies the very goal of miniaturizing all the equipment involved.

A.

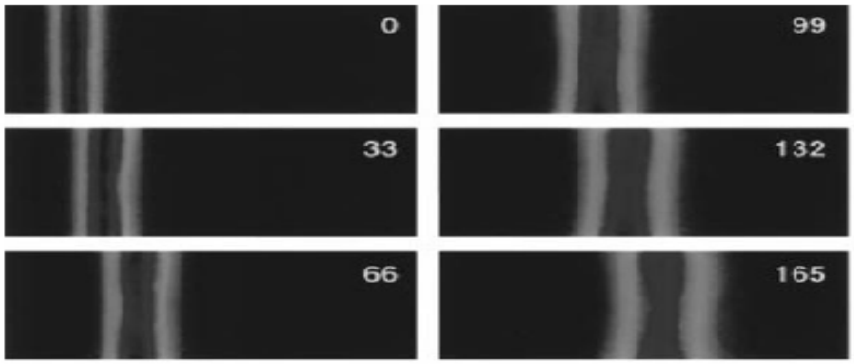

B.

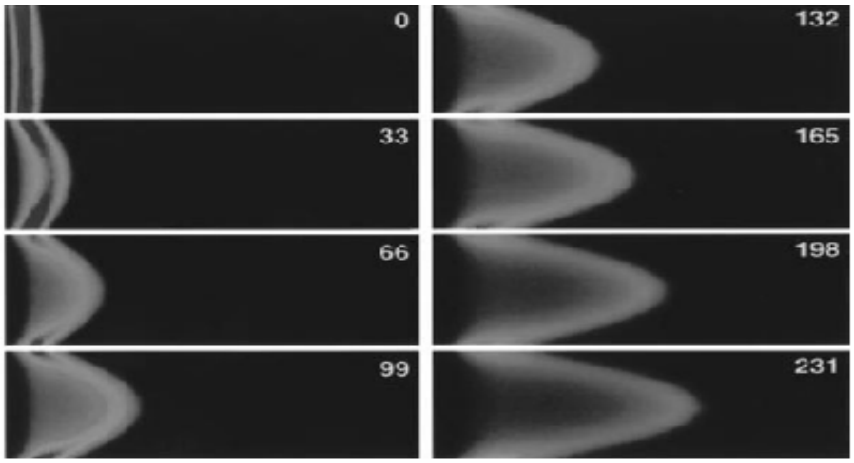

Figure 2.1 Visualization of flow profiles. (A) electroosmotic flow (EOF) and (B) pressure-driven flow [6]

Electrokinetic flow is another method of controlling fluid in miniaturized devices. Electroosmotic flow uses movement of counterions around the surface of the walls by applying electric field. Unlike pressure-driven velocity which has a parabolic profile, electro-driven flow has flat velocity profile as shown in Figure 2.1. This is due to the bulk solution being driven close to the wall or surface of the capillaries. Similar to pressure-driven system, this method also involves external macro elements attached to micro devices. These arrangements are usually complex and require multiple power supplies. In an effort to have a complete miniaturized device, the external macro elements can be avoided by using capillary action-driven flow. This passive pumping technique which doesn't require any external energy is based

on interfacial surface energy between the fluid and walls. Fluid flow is mainly controlled by the surface chemistry and channel geometries.

The wetting properties of microchannels have significant effect on this method. This concept can simply be understood from how water reacts toward hydrophilic and hydrophobic surfaces. PDMS is used in many microfluidic systems. This is due to ease of pattern fabrication, chemical stability and good optical properties which are desirable for microfluidics. While PDMS has all the qualities mentioned above, its natural property of hydrophobicity is inconvenient. This is because it is hard to attain surface tension flow in bare PDMS for most fluids used in microfluidics. Typically PDMS is treated with plasma to give it hydrophilic surface and maintain ease of fluid flow. The following section goes over details of using PDMS as well as other materials used in microfluidics.

2.2 Polydimethylsiloxane (PDMS)

In the past several years rapid microchannel fabrication has grown tremendously due to the demand in miniaturized devices and microscale flows. Silicon and glass have been materials of choice for fabrication of such devices for long time. Silicon micromachining fabrication technique is relatively inexpensive and is very amenable both to highly complex, multiplexed devices and also to mass production [17]. However, using silicon has many drawbacks including geometrical limitations. Some of these are crystallographic planes, non transparent to most wavelengths of interest for biological applications, and the process involves using complex and time consuming procedures. In recent times, different polymeric materials such as polyurethane, poly (methylmethacrylate) (PMMA), polystyrene, polycarbonate (PC), and polydimethylsiloxane (PDMS) have been used as base materials for microchannel fabrications.

PDMS is receiving an increasing amount of attention. It is initially a liquid matter which has two components: a silicone elastomer and a cross-linking or curing agent. The liquid

components are combined in various ratios but mostly 10:1 elastomer to cross-linker ratio. Once PDMS is cured, it is optically transparent which makes it suitable for imaging experiments. PDMS can cure at room temperature and cures faster at elevated temperatures [18, 19]. Special advantages of PDMS are its ability to bond well on a number of surface materials, low cost and unique properties such as transparency in the optical range of 230–700 nm wavelength, high permeability to gases, high elasticity, ease of processing [20], hemocompatibility/biocompatibility, and biologically relevant young's modulus [21]. Due to these facts, PDMS is being used as prototype for testing various microfluidic devices. Especially it has been important in the field of micromixing [22].

2.3 Microchannel Fabrication

A number of techniques have been reported for fabrication of microfluidic devices by several groups [20, 21, 23-30]. In general fabrication method can be divided in to two groups. The first is a top-down approach. This is used commonly and practiced frequently in commercial and research devices. The technique includes standard lithography, soft lithography, nanoimprint lithography, chemical etching and many similar types of techniques.

Photolithography and chemical etching are used widely for microelectronics and microelectromecanical systems [6, 31, 32]. The issue with using this type of fabrication technique is that they are expensive, require specialized tools, are complicated, and time consuming. Furthermore the end results of these approaches are rectangular shaped cross-sections of channels [33-35]. Another shortcoming is that these use harsh organic solvents that can easily harm and disturb the protein and cellular environment. Generally, photolithography shows to be difficult and pricey to use as foundation for protein or cell patterning. Soft lithography seems relatively a better method in fabricating these materials. The second is bottom-up approach. This is relatively new and much more is yet to be explored. This heavily depends on specific arrangements of natural assembly of atoms and molecules to create micro

and nanostructures [5]. In the past, bottom-up approach has been used to fabricate structures like quantum dots and carbon nanotubes [36].

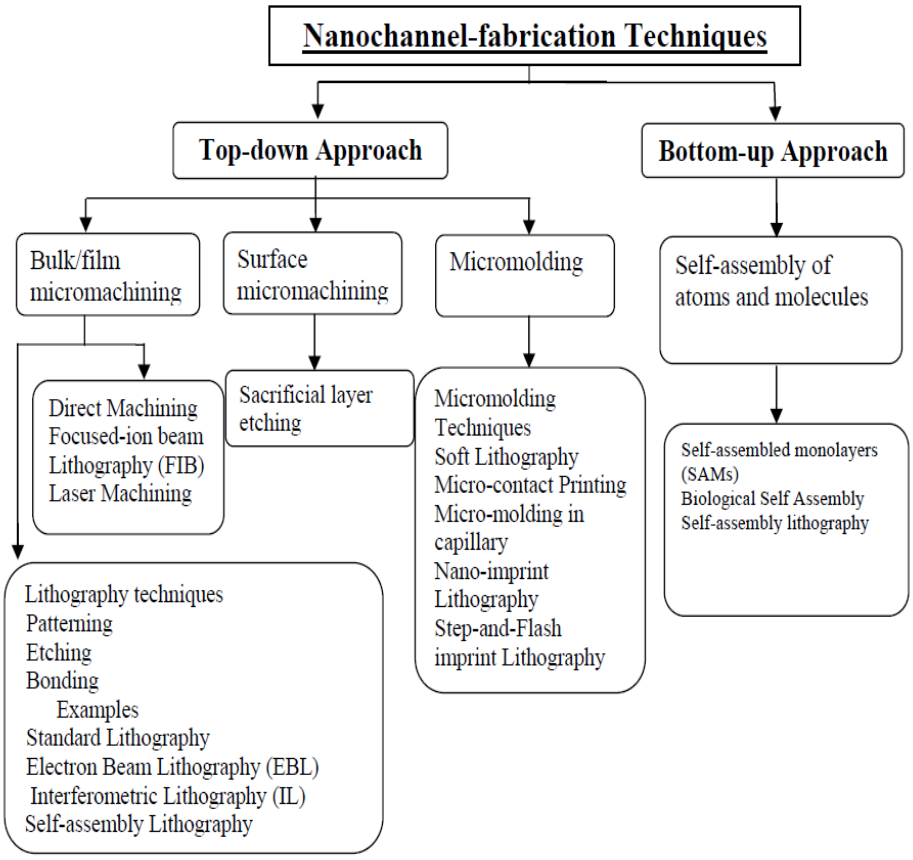

Figure 2.2 Classification of various micro and nanochannel fabrication [5].

2.3.1 Lithography

Even though photolithography is a standard method of lithography, different types of lithography processes have evolved over time. Some of these are soft lithography, electron beam lithography (EBL), ion beam lithography (IBL), nanoimprint lithography (NIL). All these processes carry some advantages and disadvantages. For example, a disadvantage of using photolithography is that it is limited to micron size and also difficult to work with preexisting

topography. On the other hand EBL and NIL fabrication methods produce nano-sized structures.

2.3.1.1 Photolithography

The first step in a typical photolithography process is spin coating of the photoresist (Fig. 2.3). It is dispensed at the center of the wafer and spun to cover the entire surface of the wafer. Next, the sample is exposed to UV light through the mask. The alignment of mask must be done by careful adjustment of mask and wafer. Each wafer must be placed in the proper position to allow the pattern to transfer. The final step is to develop the pattern. The developer is a solution that selectively reacts and dissolves the exposed resist (in case of positive resist). A bake then glassifies the resist for subsequent processing.

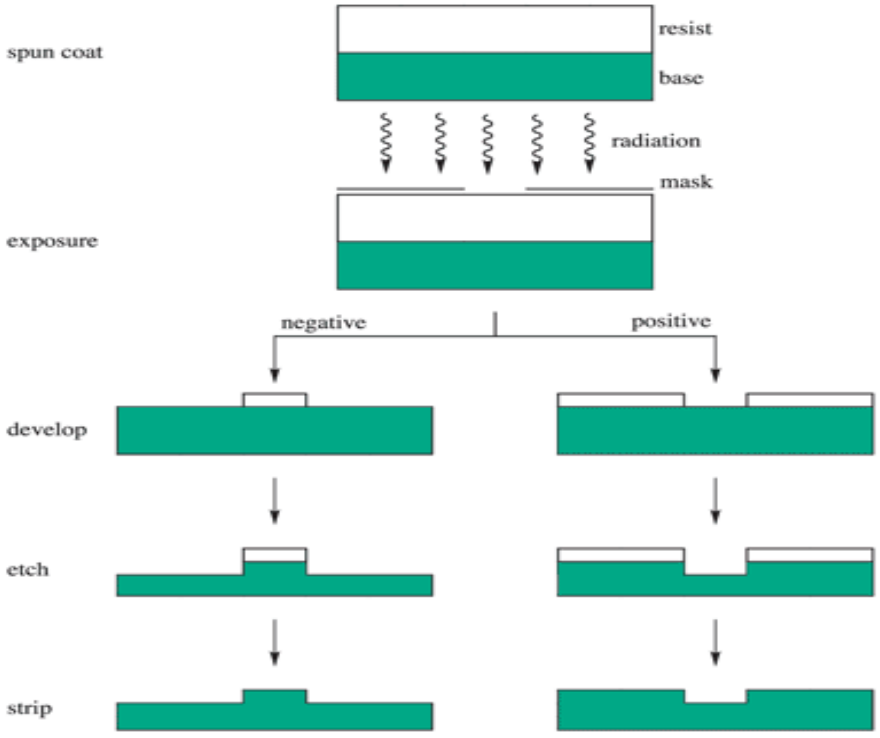

Figure 2.3 A general representation of lithographic process [2].

2.3.1.2 Electron Beam Lithography (EBL)

Electron beam lithography is similar to the basic concept of photolithography but it is a commonly used method for nanostructure fabrication. Since electrons are smaller than photons, this method has an advantage in having better resolution. The disadvantage is that it is a serial process. The process thus takes time and is expensive. Ion Beam Lithography (IBL) is a similar process to EBL except it uses ion beam instead of electron. The advantage of this method is that ions scatter less due to the weight they carry. Another advantage of using this method is that ions can directly be used to machine surface of substrate without any resist.

2.3.1.3 Nanoimprint Lithography (NIL)

Nanoimprint lithography uses completely different method of fabrication compare to the ones mentioned above (Fig 2.4). It uses mechanical pressure to define patterns in the resist on substrates. This can give high throughput to define nanoscale patterns. The beauty of this method is that micro to nanoscale structures can be patterned in parallel and the patterns can be used repeatedly. Therefore good resolution structure with relatively low cost are fabricated. With all that being said, this method is still in its development stages to improve resolution and etching resistance before it can be used in commercial applications.

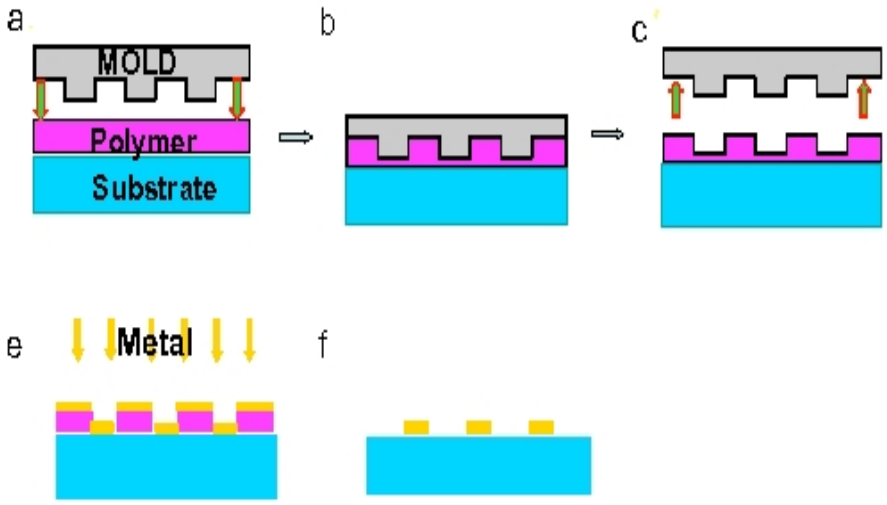

Figure 2.4 Illustration of the process of nanoimprint lithography [1]

2.3.1.4 Soft Lithography

Soft lithography is a key process for microfluidic polymer devices. In this technique, patterns are transferred to substrate differently. It provides an alternative method of fabrication of micro and nanochannels. The advantages of this method are high throughput, low cost, ease of defining patterns on a variety of substrates. As the name indicates, the patterns in this method are made out of soft materials such as PDMS. The disadvantages are reproducibility, shrinkage of polymer during curing, swelling by non-polar solvents, sagging and deformation.

Table 1.1 Advantages and disadvantages of different type of micro and nanofabrication methods [9]

Method	Advantages	Disadvantages
Bulk nanomachining and wafer bonding	• Simple concept and processing methodology • Allows for easy fluid visualization when using an optically clear cover plate or substrate • Possible to achieve stacked structures with one or more bonded substrates	• Trench depth is limited by its width to prevent trench collapsing • Requires bonding to realize device (need an additional substrate to enclose channels). • Difficulties with bonding
Surface nanomachining	• Simple concept. • Fluid visualization is possible with transparent surface layers	• Long etch times of sacrificial layer. • Upper limit of channel lengths is about 3–5 mm • Need to consider thin film stresses when fabricating channels
Buried channel technology	• Large freedom of design • Absence of assembly of wafer-to-wafer alignment steps or bonding • Surface is available for integration of electronic circuits or fluidic devices which leads to more efficient use of the substrate surface and to further overall device miniaturization • Channel shapes may be varied (pear-shaped, circular and v-grove) • Easy to fabricate nanosized channels in 2-D	• Fluid visualization is not possible • Need to develop processing technology to exploit ability to build sensors/electronics on top of nanochannels for overall device miniaturization
Nanoimprint lithography	• Low-cost process which is capable of high throughput • Mold can easily be adjusted to make large and small lateral features (nm to mm size) • Easy to fabricate nanosized channeli in 2-D	• Fluid visualization is possible if mold is fabricated from glass • Difficulty in accommodating wide ranges of feature sizes into a single mold • Lifetime of mold may be an issue

2.3.2 Self-assembly

Self-assembly refers to atomic/molecular level affinities that result into formation of nano/microstructures with little top-down intervention. A two or three dimensional component can self-assemble spontaneously in a predictable way. Recently, self-assembled structures in block copolymers are under investigation in an effort to tune the materials, properties and functions [37-39]. Different routes have been shown to tune the self-assembled structures using covalent and/or noncovalent bonds [40]. Another method of self-assembled polymeric microparticles is done through simple entropic and enthalpic interactions. This approach of fabrication method has many advantages. The process is straightforward, rapid, and involves inexpensive material to build structures.

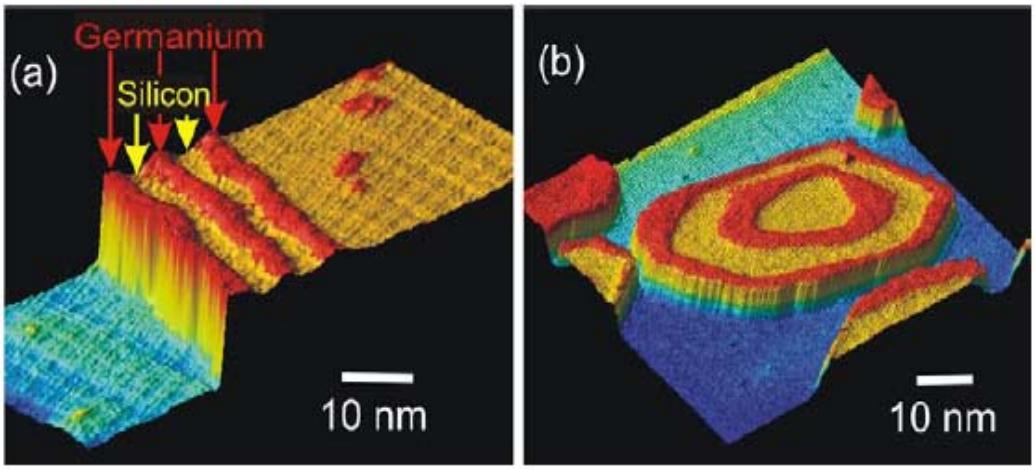

Figure 2.5 Self-assembled structures results in the formation of a nanowire [4].

2.4 Conclusion

Microfluidics has important applications in sensing, assaying, implants and more. Such miniaturized devices offer many advantages in reducing the amount of solvents, reagents and the power used to run the devices. Reaction and transport at micro/nano level also occur at higher rate compare to the macro scale systems. On top of that, the biological systems at micro/nanoscale are mimicked better using such devices. Three methods of transportation in

microfluidics were discussed in this chapter. While pressure and electroosmotic driven fluid flow techniques have their own advantages, both defy the very purpose of complete miniaturization by integrating external macro pumps. Capillary action driven fluid flow shows a promising future to be an efficient and effective method of transportation by only manipulating the surface chemistry of materials and eliminating external macro elements involved. Hydrophilicized PDMS is used in transporting fluid through micro/nanochannels and offers many advantages in microfluidics.

The purpose of this thesis is to present a novel approach to fabricate microfluidics. This chapter presents detailed background on current methods of micro/nanochannel fabrication techniques. While microfluidics are intended to reduce cost and power used to drive the device and increase efficiency, the way it is fabricated currently is costly and uses harsh chemicals that are not favorable for biochemical analysis. Lithography, which is used widely in fabrication of micro/nanochannel, involves many steps, complicated procedures and expensive equipment. Therefore another approach is needed to improve the efficiency and cost of fabrication. Self-assembly is another approach that is in its developing stages. This thesis focuses micro/nanochannel fabrication using self-assembly of particles. The technique builds up on the surface properties of materials such as covalent/noncovalent bonds or entropic/enthalpic interactions. There is a minimal need of specialized equipment and only few steps are involved in this technique.

CHAPTER 3

SELF-ASSEMBLED MICROCHANNEL FABRICATION, CONCEPTUAL FRAMEWORK AND EXPERIMENTAL RESULTS

This chapter elucidates the experimental results and scientific explanation of microchannel fabrication. Previously, researchers have explored self-assembly in various scenarios. Among these, self-assembled polymeric and non-polymeric micro/nanoparticles resulted into micro/nanochannels due to entropic and enthalpic changes of the system [3, 7, and 41]. The abundance of self-assembly in biological system to form structures at micro and nanoscales is guided by molecular interactions and thermal fluxes[8]. We use these as inspiration for our fundamental principle behind the fabrication concept. The technique presented is based on a bottom-up and non-lithography approach of microchannel fabrication. The main aim of this thesis is to define a simple, cost-effective, energy efficient and rapid approach to fabricate microchannels in polydimethylsiloxane (PDMS). The materials involved in this experiment are inexpensive and the porous membrane structures have been fabricated without any need of specialized tools. The main equipment and materials needed to fabricate the microchannels are shown in figure 3.1. A magnet is shown in figure 3.1A which is used to direct the motion of iron-oxide nanoparticles inside PDMS. This resulted in strands of particles that were aligned to each other. Figure 3.1B shows a vacuum chamber used to remove trapped air bubbles which were formed while mixing liquid PDMS and curing agent. Figure 3.1C shows the hotplate used to control the temperature. This was used to characterize temperature dependence of microchannel sizes and porosity during PDMS polymerization. Figure 3.1 (D-F) shows different hydrophilic particles used in the experiments.

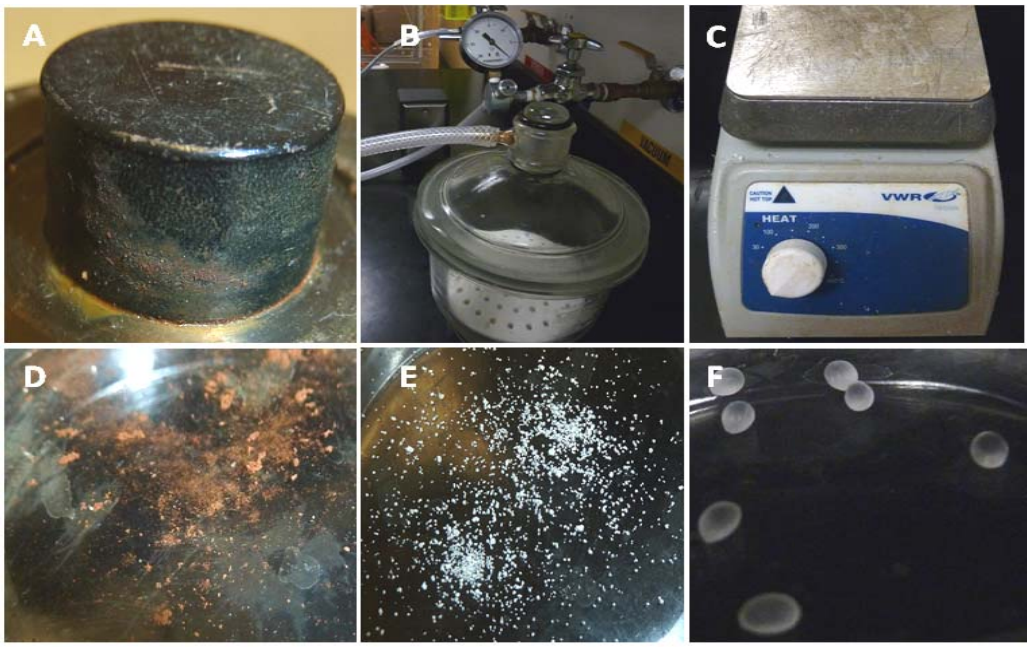

Figure 3.1 Equipment and materials used in fabricating microchannel. (A) Magnet (B) Vacuum Chamber (C) Hotplate (D) Iron-oxide nanoparticles (E) Poly Ethylene Oxide (PEO) (F) Poly Urethane (PU)

Polydimethlysiloxane (PDMS) is base membrane used in this thesis at all times. Silicon is a Group 4 (IVA) element found in the periodic table beneath carbon, and it is naturally found in abundance. It is usually found bound to oxygen as either SiO_2 or SiO_4. These are stable bonds compared to Si-Si bond, thus are more favored. These bonds can easily be opened and closed in a scissor-like fashion, giving PDMS a very elastic property. Many litratures show the outstanding mechanical properties of PDMS [42, 43]. It is optically clear, flexible, permeable to gases, inert and non-toxic. PDMS has a chemical formula of $(H_3C)_3SiO[Si(CH_3)_2O]nSi(CH_3)_3$. The number of repeating monomer unites of $[Si(CH_3)_2]$ are represented by *n*. A different physical property of PDMS is achieved by altering *n* in the chain. PDMS synthesis begins with adding dimethylchlorosilane and water together. The chemical reaction is given below:

$$n\ Si(CH_3)_2Cl_2 + n\ H_2O \rightarrow [Si(CH_3)_2O]n + 2n\ HCl$$

The chemical structure is shown in figure 3.2 by assembling the units of this polymer chain in a network of polymer. The vinyl group is present at each end for a long PDMS polymer chain. The PDMS chains are linked by a short crosslinker. In this thesis, the PDMS network was synthesized by mixing the base elastomer and curing agent. The mix can be prepared using different ratios. This provides strength of cross-linking. If the curing agent is smaller, the degree of PDMS network cross-linking is less. This forms a softer and more flexible PDMS network. On the other hand, when the curing agent is used in a higher ratio, the sample is stiffer because of the formation of the high degree of cross-linking. Even though 10:1 was the ratio between base polymer and curing agent for most of the cases in this thesis, other ratios were also experimented to analyze the effect they had on the formation of micro/nanochannels.

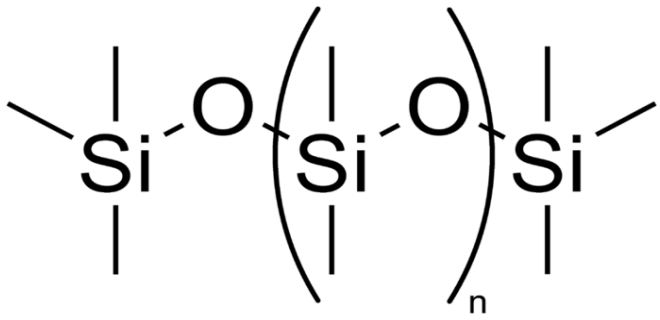

Figure 3.2 Chemical formula of PDMS

3.1 Fabrication Concept

3.1.1 Phase Separation

The fabrication method shown here is based on intense repulsive interactions between the hydrophobic PDMS and hydrophilic particles. This results in phase separation during the polymerization process. Repulsive interactions between dissimilar molecules lead to phase separation of the two molecular species. A typical example of this phenomenon is evident in

mixture of oil and water. A clear separation of these two molecules due to interface of the opposite property is obvious if they are not vigorously mixed. Phase separation is best summarized in Figure 3.3. Parameters such as the relative proportions of molecules or thermodynamics rules determine the stability of a mixture [8]. Symbols given in a Figure 3.3 are defined as following:

X- Repulsive molecular interactions

K_B- Boltzmann's constant

T- Absolute temperature

Φ- Volume fraction of one molecule in the mixture

It has been reported earlier that the process of phase separation is the repulsion of a thermodynamically unstable solution [44]. The mixture is considered stable when X is small compared to K_BT. When Φ value is 0 or 1, it represents pure sample of molecule A or B. At 0.5, it represents a one-to-one mixture of A and B. Figure 3.3 illustrates the relationships between temperature, composition and stability of a mixture. In the graph, the solid curve divides the phase diagram into homogeneous and heterogeneous regions. Above the solid curved line, it is considered homogenous mixture. Below this line, it is heterogeneous mixture where components are separated in their own region. A formation of bicontinuous channels of each material result in a mixture below the dashed curve. These are unstable and will be phase separated by spinodal decomposition (SD). Mixtures between the spinodal line and the phase boundary are metastable, and can be only phase separated through nucleation and growth (N+G).

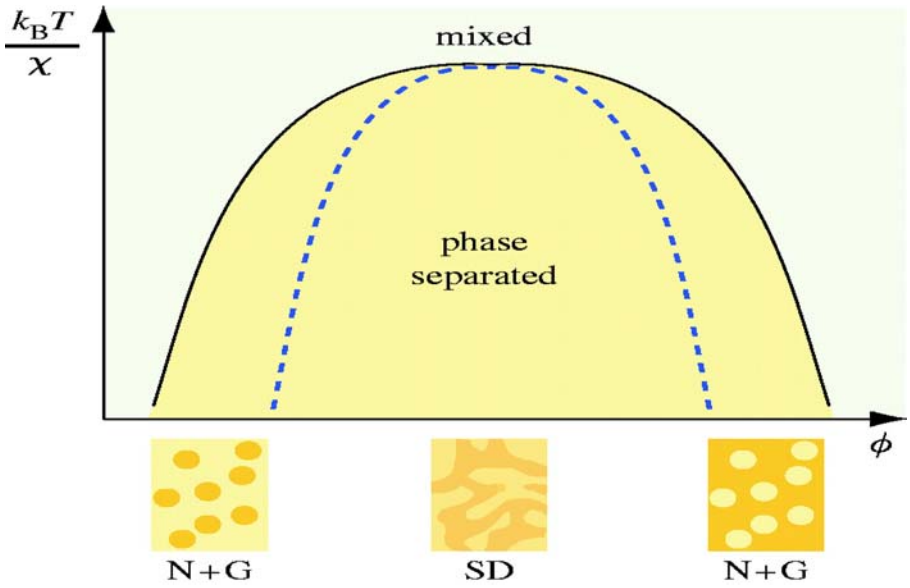

Figure 3.3 A schematic phase diagram showing the relationship between the temperature , composition, and the stability of a mixture [8]

The mixture of hydrophilic particles with PDMS falls between solid curve and the dashed line where there is nucleation. Directional polymerization of PDMS pushes the hydrophilic particles from bottom-up (Fig. 3.4). The phase separation occurs when free energy of two compounds mixing is greater than zero.

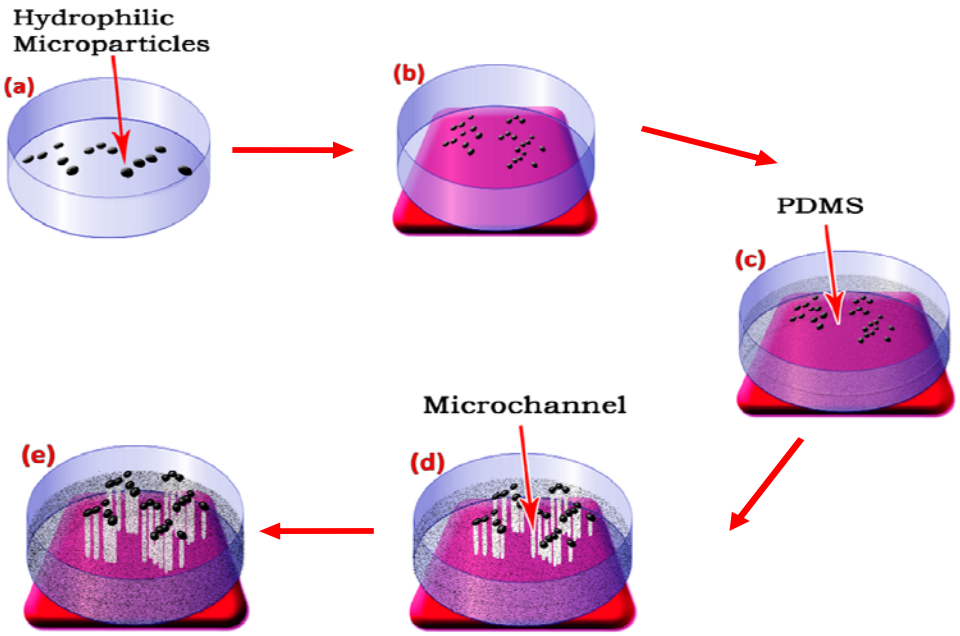

Figure 3.4 Schematics depicting steps for fabrication of microchannels in PDMS using hydrophilic particles. Read plate denotes hot plate. (a) Hydrophilic particles before exposure to heat (b) Hydrophilic particles after expose to heat (c) PDMS poured on the top of hydrophilic particles (d) PDMS starts to polymerize and hydrophilic particles migrate forming microchannels along the way. (e) PDMS fully polymerizes with in situ growth of microchannels.

3.1.2 Entropy and Enthalpy

Free energy determines how well two compounds mix to form a solution. This is a resultant effect of enthalpy and entropy as shown in equation 3.1 below.

$$\boldsymbol{\Delta G = \Delta H - T\Delta S} \tag{3.1}$$

Past experiments demonstrate that particles can be entropically driven to self-assemble into 3D polymer prior to complete cross-linking when surface energy forces are properly tuned [45]. Entropic forces were putatively the main reason that led to the migration of nanoparticles in the solid substrate [46]. The justification was that the interaction between the translational entropy of the drops and the configurational entropy of the polymer connections created an interface between them and becomes the driving force for the phase transition [47]. Based on this, it is predicted that hydrophilic particles' random movement and collision driven by entropy lead to

ejection of particles out through the PDMS matrix. It is important to understand the magnitude of the thermal input which will play a critical role in the final outcome of the membrane. On a PDMS based polymer, the decrease in entropy is a result of polymerization which reduces the number of configurations that molecular sub-units can have [48, 49] . During polymerization, the cross-linking reaction increases which decreases the entropy of the system. The molecular weight and the macromolecular network extend to the whole sample and coexist with loose branched networks that are not yet part of the network. This is known as the gel-point [7]. Particles immersed in PDMS during polymerization don't get intercalated during gelation [50]. The method of fabrication presented here is based on this idea where repulsion forces of hydrophilic/hydrophobic interface are used to leverage the immiscible particles to be pushed out of PDMS during polymerization. The opposing interfaces and applied heat increases the mobility of cross-linking sub-units, while gelation reduces entropy of the system while PDMS is cross-linked. This phenomenon allows the system to self-assemble from bottom-up in such a way that hollow microchannels are formed.

3.2 Evidence of the Concept

Figure 3.5 is a simple demonstration of the basic principal of interface of hydrophobic/hydrophilic liquids undergoing a phase separation process. At the beginning, blue ink was homogeneously mixed in the liquid PDMS. Once it was well mixed, the homogeneous solution was placed on the hotplate and exposed to heat. Initially, all hydrophilic particles, drops of blue ink in this experiment, attracted each other and formed a cluster. Phase separation occurred when PDMS started to cross-link, creating tight and dense networks from bottom-up. The process pushed the hydrophilic clustered layer to the top (Fig. 3.5(C)).

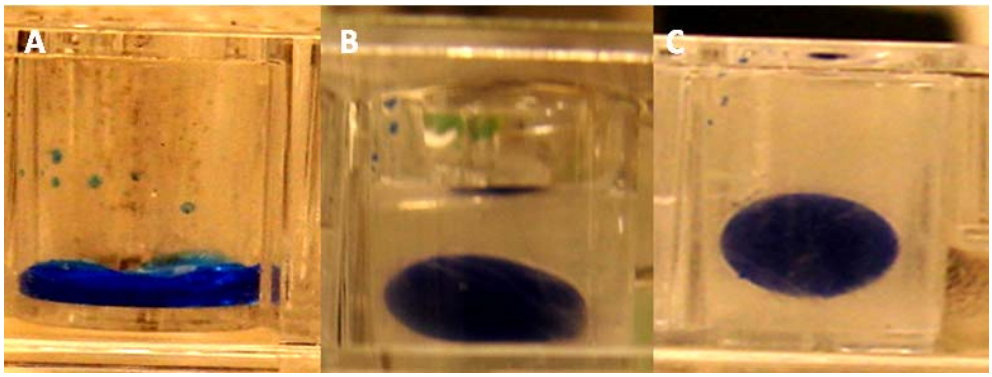

Figure 3.5 Photomicrographs of hydrophilic ink droplets pushed from bottom up while PDMS is polymerizing. (A) Blue Ink in a well, (B) Ink clusters in hydrophobic environment of PDMS, (C) Lift-up of round ball on heating when PDMS is heated from the bottom [3].

In a similar manner, hydrophilic iron-oxide nanoparticles were used in experiment instead of the blue ink to see if they are expelled through the hydrophobic network of PDMS during polymerization. The mixing of iron-oxide particles and PDMS was a heterogeneous process. Therefore, individual particles or small clusters of the particles were found unlike the blue ink which forms one big cluster. Figure 3.6 shows the SEM micrograph of iron-oxide nanoparticles on the surface of PDMS, where the mobility of the nanoparticles in this case was from the bottom-up. The nanoparticles surfaced on the top of PDMS [7]. This was the result of the force exerted by the hydrophobicity on the hydrophilic nanoparticles.

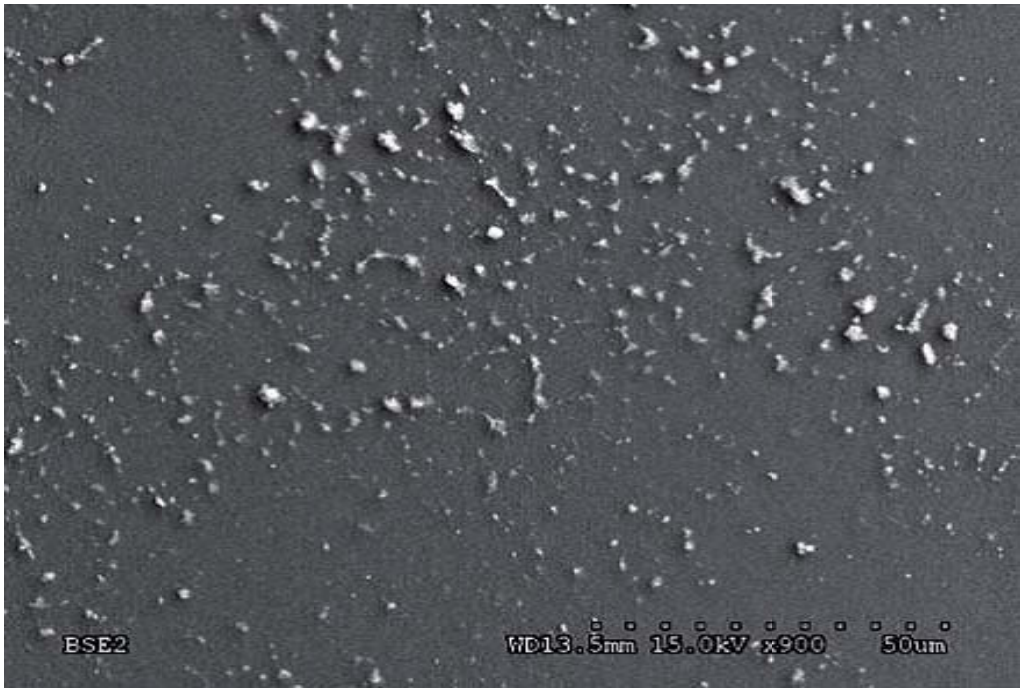

Figure 3.6 SEM micrograph of iron-oxide nanoparticles on the surface of the PDMS [7].

This behavior depicted simple particle interactions in the PDMS membrane. Using optimum temperature and parameters like curing agent concentrations and magnetic field, hydrophilic particles were pushed out leaving circular hollow channels behind.

3.3 Non-Polymeric Hydrophilic Particles

This section goes over micro/nanochannel formation using different types of hydrophilic particles. Channel formation was controlled by manipulating different parameters such as temperature, curing gent, and magnetic field. The particles produced micro/nanochannels with pore size ranging 500 nm -1 mm. Each section goes over the different type of hydrophilic particles used, the protocol followed, results found, and characterization of pore size and porosity of the membrane.

3.3.1 Vaporized Particles

This particular experiment was something that was discovered at the early stages of this project. When pure PDMS was placed in a clean Petri dish or on glass slide and exposed to

heat, there was no channel formation throughout the membrane. However, it was interesting to observe that a drop of pure PDMS which was placed directly on the hotplate with high temperature had abundant channels. This was due to the topography of the hotplate which led to trapping of humid air particles between the PDMS and the hotplate. Humid air contains water vapors[51] which are of course repelled by hydrophobic PDMS. The temperature applied increased entropy of the trapped vapor particles while entropy of PDMS decreased due to formation of tight network. The hydrophilic vaporized particles are dynamic due to the force of the hydrophobic environment that surrounds them. Direction of particle's motion is guided by law of thermodynamic which favors low entropy. This process pushes particles from bottom-up which leaves behind a track of hollow channels resulting in porous PDMS membrane. Using this approach further experiments were performed applying various parameters such as temperature and curing agent to characterize channels. The protocol followed in producing such porous membrane is explained below.

PDMS prepolymer (base:curing agent in the ratio 10:1) was poured in a clean glass beaker and vigorously mixed. It was then placed in vacuum chamber at 25 psi for degassing. This PDMS prepolymer was gently transferred on to a clean glass Petri dish for curing with the hydrophilic moiety under investigation already placed in the dish. In this case, the PDMS was directly poured on a hotplate for polymerization, at different temperatures. The rough topography of hotplate surface contributed to trapping of vaporized particles immediately after PDMS came in contact with the hotplate. The vaporized particles went through phase separation during PDMS polymerization from the bottom-up leaving empty tracks behind. This resulted in abundant number of well aligned circular microchannels throughout PDMS membrane.

The porosity and pore size of this phenomenon were heavily dependent on two parameters, temperature and concentration of curing agent. Figure 3.7 shows the irregular pore

size formation using curing agent concentration of 10%, 20% and 30%. It is illustrated that increasing concentration of curing agent led to decreasing pore sizes. This was because the higher concentration of curing agent strengthened the cross-linked PDMS. This tight network reduced the ability of the vaporized particles to expand farther. Therefore, vaporized particles were confined in smaller spaces.

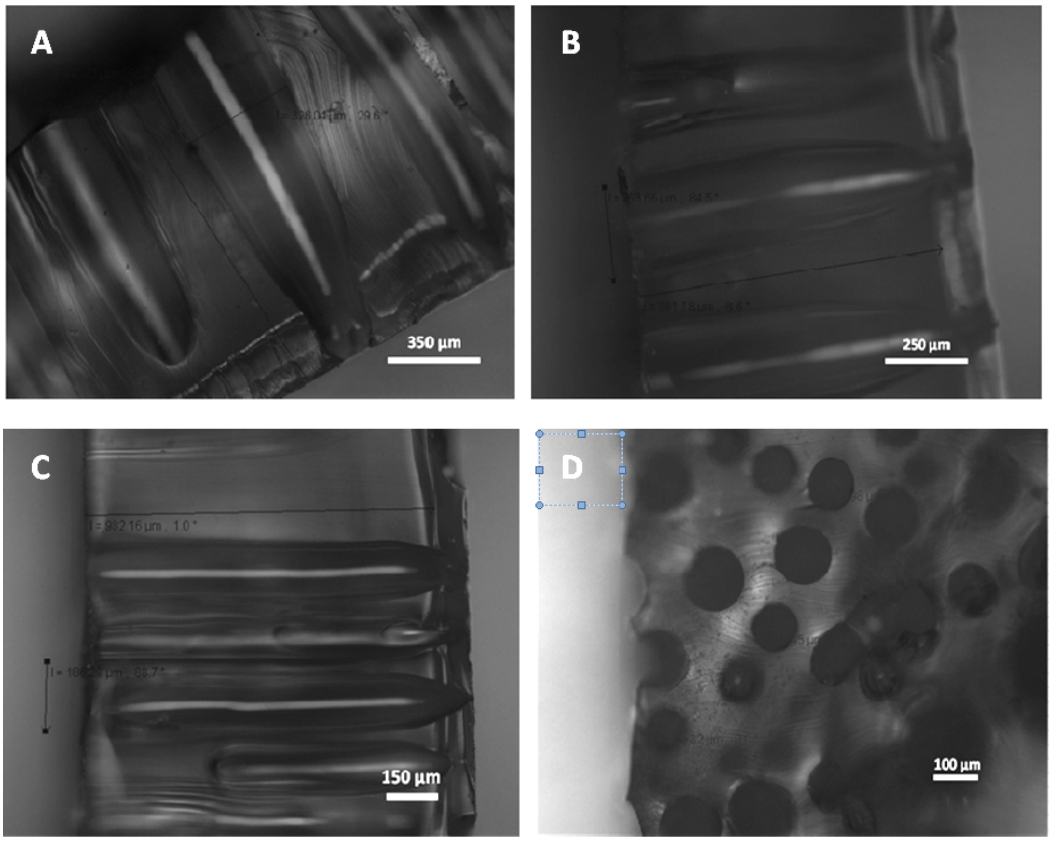

Figure 3.7. Cross sectional views of channels formed using direct polymerization technique with various curing agent concentrations (A) 10%, (B) 20%, and (C) 30 % PDMS. (D) Top view of channels formed in 30% PDMS.

A similar relationship was also discovered when characterizing pore size against temperature ranging from 100 to 175 °C. Channel diameters tended to decrease when temperature increased. The reason for this phenomenon is that as temperature increased, rate of polymerization increased as well. This resulted into rapid PDMS cross-linking which

decreased the time it took for vaporized particles to expand. On the other hand, number of pores increased when temperature increased. At lower temperatures, PDMS solution had time to slowly fill up any air pocket present between the thick viscous solution of PDMS and the surface of hotplate. This resulted in nonporous membrane. However, increasing the temperature gave less time for the viscous solution to move and high number of pores were formed (Fig. 3.8).

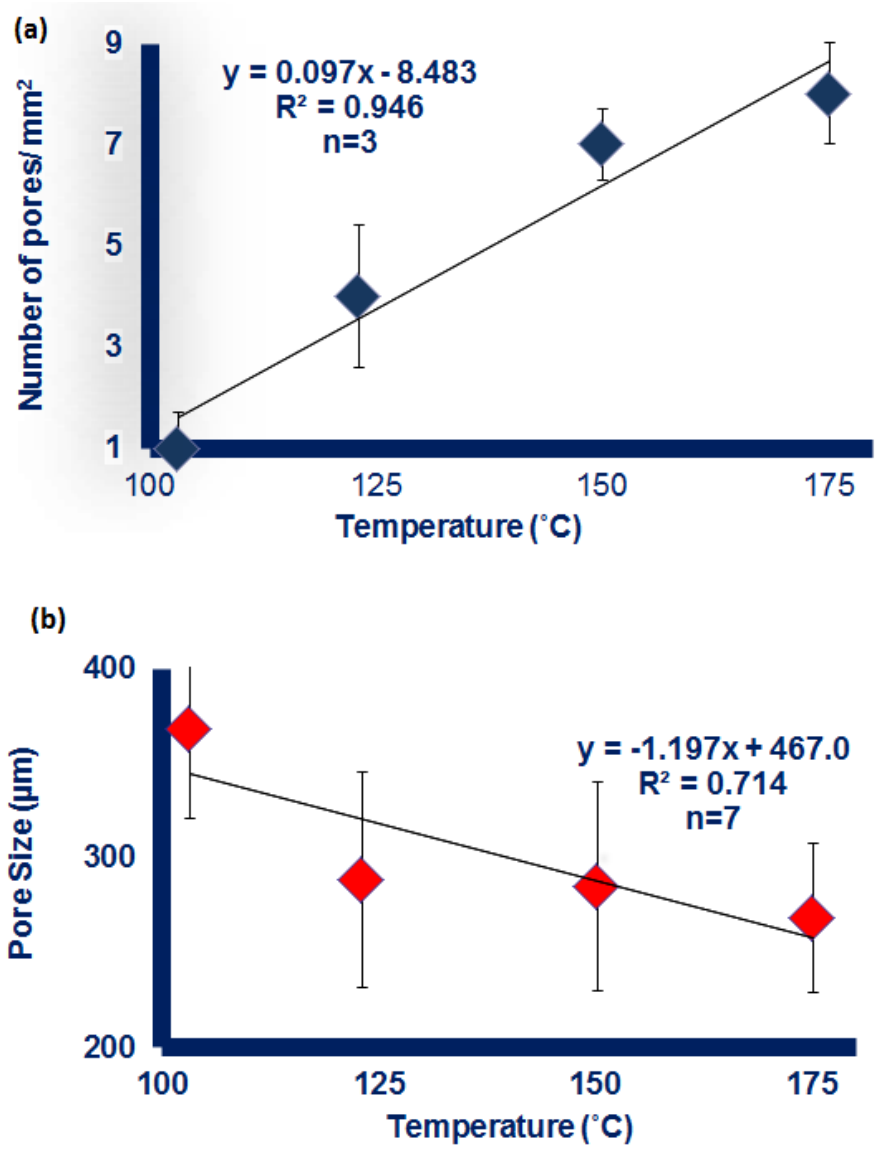

Figure 3.8 Effect of temperature on pore size and porosity. (A) A linear relationship between porosity and temperature. (B) Inverse relationship between pore size and temperature.

3.3.2 Acetone

Acetone is a volatile hydrophilic substance which was used as alternative to induce microchannels formation. The general procedure of this technique starts with preparing mixture of liquid PDMS with curing agent at 10:1 ratio as mentioned earlier. Acetone is then added to

the mixture and stirred well. The mixture must be degassed before polymerizing to remove any air bubble formed during stirring. Even though some percentage of acetone is lost due to the volatile nature of the solution, degassing is vital to ensure fabrication of homogenous membrane. While the heat polymerized the PDMS, it increased the entropy of acetone molecules similarly as seen in the vaporized particles experiments. This led to penetration of the cross-linked PDMS and generation of hollow channels throughout the membrane. In previous work, it was reported that channel formation of such technique resulted in porous membrane at low temperature [3]. The experiment used 25% of acetone mixed with PDMS. This was degassed and a thin layer of the polymer was made over a glass slide and cured at 80 °C. This phenomenon led PDMS network to self-assembled and form pores with diameters ranging between 10-20 μm. (Fig. 3.9)

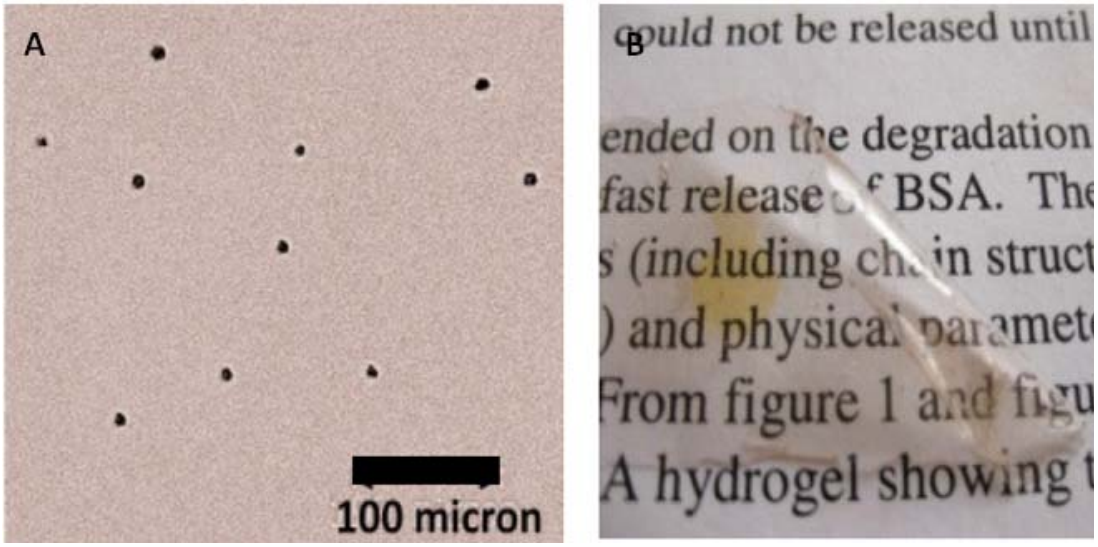

Figure 3.9 PDMS membrane made using acetone. (A) Optical image of porous membrane (B) Optical image showing the transparent membrane [3].

Different percentages of acetone (1%, 2%, 3%, and 4%) were mixed to PDMS. After all air bubbles were removed using vacuum chamber, the mixture was poured in Petri dish and placed on the hotplate for curing. The temperature was kept constant at 275 °C for all experiments. The results exhibited similar type of channels as those of vaporized particle

experiment. The pores sizes increased as the percentage of acetone increased. This method was used to control pore size while maintaining constant temperature. The relationship between the percentages of acetone to pore size is shown in Fig. 3.10.

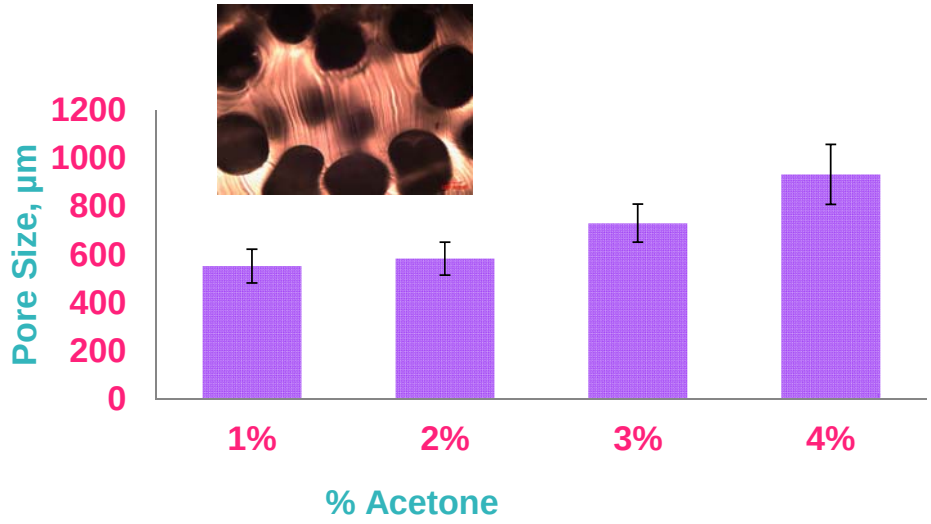

Figure 3.10 Acetone molecules penetrate through cross-linked PDMS resulting in microchannels formation at 250ºC. The graph shows the relationship between acetone percentages to pore sizes.

3.3.3 Iron-oxide Nanoparticle

Hydrophilic iron-oxide nanoparticles with diameters around 30 nm were also used alongwith magnetic force for micro/nanochannel formation. The PDMS was mixed with the curing agent and degassed as mentioned before. The nanoparticles were placed spread out on a Petri dish. The PDMS was then poured on top of the nanoparticles carefully and the Petri dish was placed on hotplate for polymerization. During polymerization, a magnet was placed on the top to give directionality to nanoparticle travel through the curing PDMS. Particles traveled upward toward the magnet as shown in figure 3.11. The schematic diagram shows the general process of this technique.

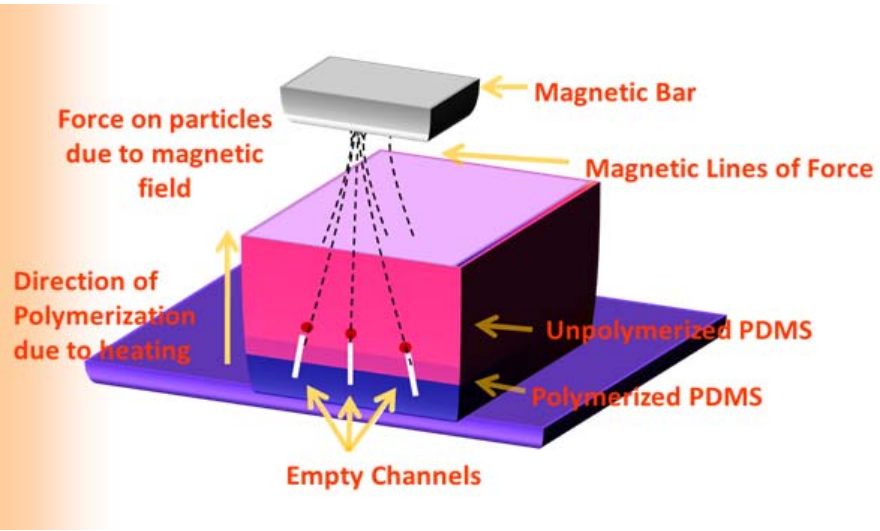

Figure 3.11 Schematic of magnetic field effects on iron-oxide nanoparticles movement in PDMS [3].

Apparent signs of channel formation were observed using this technique. The particles that traveled at the same rate as the polymerization rate left traces of channel formation behind. The channel diameters ranged between 500 nm to 25 μm even though particles used had diameter of 30 nm. This was due to the aggregation of the nanoparticles prior to polymerization. It was also observed that not all the particles produced channels. Some of the particles came out of the PDMS without creating any channels. These were mostly the particles that were placed close to the magnet. The speed of travel for these was faster than the rate of PDMS polymerization. Thus, the particles were pushed out of the polymer without leaving channels behind. In some cases, the particles were observed to be embedded in the middle of the membrane. These particles were placed far from the center of the magnet field therefore traveled slower than the rate of PDMS polymerization. Consequently, the particles were trapped during PDMS polymerization and were not able to travel farther. The results found using iron-oxide nanoparticles are presented in figure 3.12.

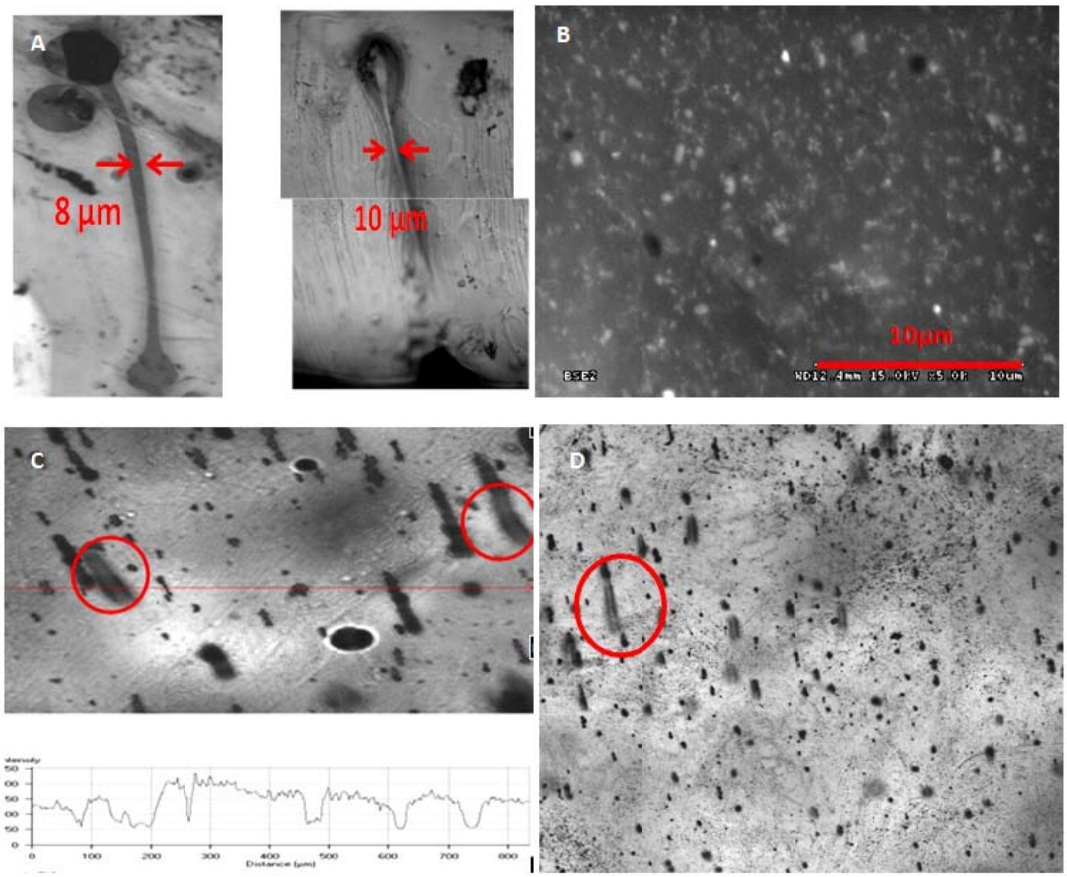

Figure 3.12 (A) Confocal micrographs of channels formed by iron-oxide particles showing 8 and10 µm diameter channels [3]. (B) SEM micrographs of pores in the PDMS membrane made using iron-oxide nanoparticles with 500 nm diameters [7]. (C) and (D) Confocal photomicrographs of iron-oxide nanoparticles traveling from bottom to up away from the hotplate. The red circle indicates hollow channel formation.

3.4 Conclusion

The science behind the fabrication method and results are discussed in this chapter. The purpose of this technique is inspired by nature's self-assembly of atoms and molecules to form micro and nanostructures that provide important functions in a biological system. The technique shows an approach of non-lithography that builds particles from the bottom-up using bench-top tools. Images of these materials are shown in this chapter and their use is discussed.

The self-assembly of the microchannels reported in this thesis is based on intense hydrophobic and hydrophilic interactions of particles. Hydrophobic PDMS and hydrophilic microparticles and nanoparticles were used to create the opposite force. This force between particles led to phase separation during PDMS polymerization. During the phase separation, hydrophilic particles traveled from the bottom up leaving empty and hollow channels that were parallel to each other. Entropic and enthalpic interactions also played important roles in the way micro/nanochannels were self-assembled. When heat was applied to hydrophobic and hydrophilic particles, both responded differently. Entropy of PDMS decreased when heat was applied due to polymerization which formed a tight network from the bottom-up. On the other hand, entropy of hydrophilic particles increased with increasing temperature. High temperature set hydrophilic particles in motion from the bottom-up and polymerized PDMS. This opposite effect resulted in the formation of hollow channels throughout the membrane. The theory was validated using two simple experiments by mixing blue ink and iron-oxide hydrophilic particles with PDMS. Both of the hydrophilic particles surfaced to the top of the PDMS membrane due to the opposite forces between hydrophobic/hydrophilic materials and the enthalpy/entropy change in the system.

Three non-polymeric hydrophilic particles were tested in experiments. Vaporized hydrophilic particles formed abundant channels throughout PDMS membrane. Pore size and porosity were characterized using different percentages of the curing agent and temperatures. Pore size decreased linearly when the percentage of curing agent and temperature increased. However when the temperature increased, the number of pores increased. Acetone driven channels were dependent on the temperature and the ratio between acetone and PDMS. Increasing acetone increased channel diameter depending on the temperature applied. Iron-oxide nanoparticles also exhibited hollow channels formation. These particles were used along with a magnetic bar for direction and alignment of channels. For iron-oxide experiments,

channels were bigger than the diameter of particles used due to the aggregation of hydrophilic particles which formed clusters. Channel diameters from 500 nm-900 μm were formed using these hydrophilic particles.

CHAPTER 4

POLYMERIC HYDROPHILIC PARTICLES

4.1 Microchannel Formation with Poly (ethylene oxide) and Polyurethane

Chapter 3 showed formation of micro/nanochannels through interface of non-polymeric hydrophilic particles. In this chapter, self-assembly of microchannel through interactions of polymeric hydrophilic particles with polydimethylsiloxane (PDMS) are discussed. Poly (ethylene oxide) (PEO) and polyurethane (PU) are the two polymeric hydrophilic particles explored in this chapter. Self-assembly of microchannels occurred when hydrophilic PEO/PU were covered with hydrophobic PDMS as it cross-linked. The PEO/PU particles were pushed out of the bulk PDMS. While PEO/PU particles were being pushed out, these left empty tracks behind. PEO depicted ease of handling, better inherent alignment and excellent repeatability. The following are the major discussion points of this chapter.

- Fourier transform infrared spectroscopy and optical/confocal laser scanning microscopy to characterize the fabricated channels.
- Dependence of diameter, arrangement and height of the channels on curing temperature.
- Self-assembled formation of concentric circular arrangements of molten polymer.
- The flow behavior of ink solution to measure flow and micromixing characteristics in the microchannels.

4.2 Experimental Methods

Two major procedures were followed in the experiments. The first batch of experiments dealt with fabrication of channels using PEO and PU. Various techniques were used to fabricate channels with different size and length. The second set of experiments showed microfluidic flow

and micromixing using the fabricated microchannels. Capillary driven fluid flow was carried out through one opening and through channels, and measurement of velocity profile was carried out.

4.2.1 Fabrication of Microchannels

Commercial grade PEO powder and PU beads, both hydrophilic in nature, were used in the experiments. PEO powder was composed of microparticles and PU beads sizes were between 2.5-3.5 mm. Both PEO and PU are hydrophilic. PDMS was prepared in the same as explained mentioned in chapter 3. The steps of these experiments are as following:

A. The base was mixed with the curing agent in a ratio of 10:1 and stirred vigorously for several minutes until the curing agent was homogenously mixed.
B. Degassing was performed by placing the mixture in a vacuum chamber at 30 psi until all trapped air was removed.
C. Experiments for PEO microparticles were on a pre-heated Petri dish. Ten micrograms of the PEO microparticles were placed spread out on Petri dish with temperature between 200-400 °C.
D. At these temperatures PEO microparticles completely transitioned to molten and viscous fluid within a few seconds and started to evaporate.
E. PDMS (2-3 g) was poured on the top of the viscous PEO film. The opposite affinities of PEO and PDMS made pouring of PDMS very critical.
F. The pouring of PDMS in the Petri dish on the top of the molten microparticles was thus a key step which influenced the final sizes and positions of microchannels.
    i. When PDMS was poured from one side to another by gradually laying it over the Petri dish, the microparticles were not disturbed and initial position remained intact.

ii. On the other hand if PDMS was poured at just one position spreading in expanding circular pattern, the molten PEO moved away from the center.

G. The different characteristics of microchannels evolved as a result of different pouring techniques. Polymerization process took from a few seconds to about 2 minutes depending on the temperature used. Once PDMS was fully polymerized, the Petri dish was removed from the hotplate and was allowed to cool down to room temperature.

H. The same steps mentioned above, A- G, were used to perform experiments for PU beads with exception that PU was replace instead of PEO. A few beads of PU (6-8) were used for each experiment

I. For characterization, channels were sliced open to measure pore sizes. It was also sliced from top to bottom to measure the length of channels. Confocal and optical micrographs of channels were taken and analyzed. Furthermore, Fourier transform infrared (FTIR) spectra were done for PEO, PU, pure PDMS, and the porous membrane fabricated in PDMS.

4.2.2 Fluid Flow Experiment

Fluid flow experiment with through channels and channels open from one side only were performed. Since PDMS is hydrophobic it was important to treat the surface with plasma before fluid flow experiments. The fabricated microchannels were treated with plasma for 15 minutes for characterization of fluid flow using capillary action. The steps for three experiments performed for fluid flow in the microchannels are given bellow.

A. First experiment was carried out by opening only one side of the channels. The open sides of the channels were placed down inside a blue ink solution to trace fluid motion inside channels. Once fluid transferred to the channels of

membrane, the channel membrane was removed and placed in a red ink solution. This experiment was performed to analyze two fluids flow using same inlet.

B. In the second experiments, channels were cut open from both sides and membrane was placed horizontally. Red and blue ink drops were placed on opposite ends of the channels using a syringe. Fluid motion was observed and analyzed using optical micrographs.

C. In third class of experiments, a 300 μm channel was cut open from both sides and a red drop was placed on one opening using a syringe. A quick penetration of liquid was observed. This time was defined as *t*=0. The capillary action sucked in the fluids. The fluid motion was observed with optical microscope, flow rate analyzed and the velocity of fluid inside microchannel was calculated by measuring distance traveled against time.

4.3 Results and Discussion

4.3.1 Characterization of Surface Chemistry

This experiment was done to analyze the composition of fabricated channels. Figure 4.1 shows FTIR spectra of PEO, PU, PDMS, and membrane formed by PEO/PU interactions with PDMS. PEO and PDMS are polymers with molecular structure $HO\text{-}CH_2\text{-}(CH_2\text{-}O\text{-}CH_2\text{-})_n\text{-}CH_2\text{-}OH$, and $CH_3[Si(CH_3)_2O]_nSi(CH_3)_3$, respectively. The most concentrated absorption peaks located for PDMS were at 387 cm^{-1} attributable to Si-O rocking mode, 791 cm^{-1} to $Si\text{-}CH_3$ bending mode, 1014 cm^{-1} to Si-O stretching vibration, 1258 cm^{-1} to $\text{-}Si\text{-}CH_3$ stretching vibration and 2958 cm^{-1} to $–CH_3$ asymmetric stretching mode [52, 53]. A peak at 1113 cm^{-1} indicated C-O stretching, 2889 cm^{-1} to $–CH_2$ stretching vibration and 1470 cm^{-1} to $–CH_2$ scissor, all these were inherent to PEO only. It is important to note that samples of PDMS membrane fabricated using PEO showed vibration modes associated with PDMS only. This showed the absence of PEO from the porous membrane after

generating the channels. Similar to PEO results, porous membrane fabricated using PU has a result similar to PDMS. Figure 4.1(b) shows that peaks related to PU were not found on the PDMS membrane made with PU. For instant, the absorption peak at 3302 cm^{-1} is due to urethane (N-H stretch) stemming from PU. PDMS membrane fabricated using PU doesn't show this and other peaks of PU. It only shows bands associated with PDMS. The result indicates that PDMS and porous membranes fabricated using PDMS/PEO, and PDMS/PU had similar FTIR results whereas PEO and PU had absolutely different peaks. As a result the membranes were composed of PDMS only. The importance of this finding is that original property of PDMS such as elasticity and transparency and chemical compositions are not altered.

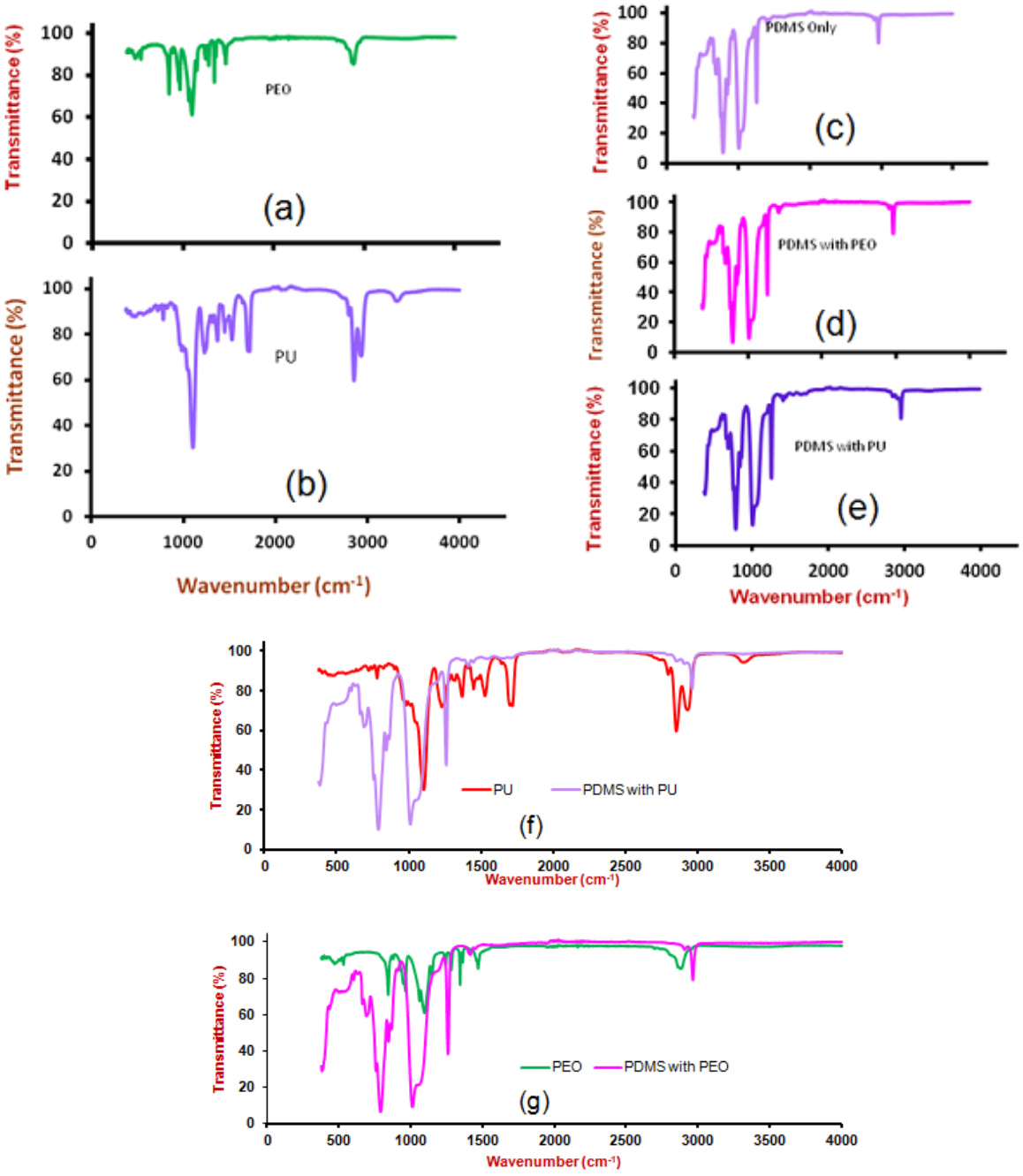

Figure 4.1 Fourier transform infrared (FTIR) spectra of (a) PEO (b) PU (c) PDMS only (d) PDMS membrane fabricated using PEO (e) PDMS membrane fabricated using PU (f) Comparison of PU and PU driven PDMS membrane (g) Comparison of PEO and PEO driven PDMS membrane

4.3.2 Characterization of Porosity and Pore Size

Optical and confocal microscopies were used to characterize channels fabricated. Figure 4.2 (a) and (b) show channels formed in PDMS driven by PEO and PU, respectively, which are both hydrophilic polymers. Circular contoured pore formation is apparent from these cross-sectional photomicrographs. Side views of hollow microchannels that were closed from both ends are also shown on the top right corners of Figures 4.2 (a) and (b). Channels generated using PEO tended to depict smaller diameters than PU particles. At 300 °C, PU driven channels had diameter almost twice of PEO driven channels. After melting at 300 °C, PU was more viscous than PEO. The inter-molecular force of attraction was weaker when the solution was less viscous. In the case of PEO, when PDMS was poured on the top and the weaker attraction between molecules resulted into smaller clusters that resulted in smaller and higher number of microchannels compared to PU induced channels. Number of pores and pore size were interdependent in each case. When pores were small, there was more PDMS bulk space available for more number of channel formations. However when pore was big, hollow space dominated and number of channels in a given area were small. PU being more viscous formed bigger clusters resulting in larger channel diameters. Figure 4.2 (a) and (b) exhibit higher number of channels formed for PEO than PU. Confocal laser scanning microscopy (CLSM) images (Fig. 4.2(c) and 4.2(d)) show the depth of PEO driven microchannels through 3D reconstructions. The images also show that deeper channels are represented by intense color like red and pink.

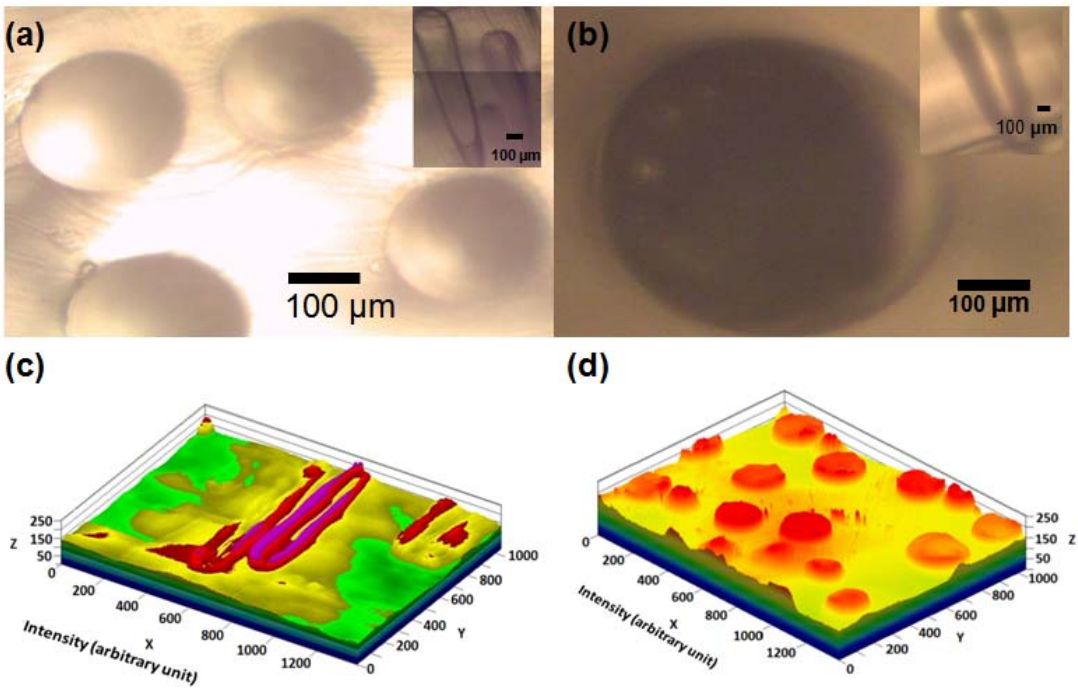

Figure 4.2 PEO and PU driven microchannels. (a) PEO driven channels (b) PU driven channel. Insets of (a) and (b) show the length of the microchannels. (c) and (d) Confocal laser scanning microscopy (CLSM) of PEO driven channels. (c) Shows cross-section along the channel length while (d) shows top view.

Table 4.1 Relationship between Temperature, Porosity and Pore Size

Temperature (°C)	# of Pores	Average Pore size (µm)
225	0	0 ± 0
250	3	69 ± 1.2
275	13	60 ± 16
300	38	34 ± 11

4.3.3 Temperature Dependence

The porosity of the membrane and the PDMS pore sizes also showed a dependence on the PDMS curing temperature. The data of Table 4.1 show channels that were cross-sectioned close to the bottom of the membrane. It was observed that when PDMS membranes were cured at higher temperature, pore sizes decreased and number of pores increased. The smallest diameter was recorded at the highest temperature. At higher temperatures, the intermolecular bonds were weak and solution became less viscous. This formed smaller but many more clusters that resulted in many more channels formed with much smaller diameters. Figure 4.3 shows channels that were cross-sectioned close to the top surface of the membrane. Here it shows both pore sizes and porosity increased with increasing temperature. The data of table 1 and figure 4.3(a), although seemingly contradictory, in fact shows the size of pores at different planes in the PDMS membrane. At the bottom of the membrane (Table 4.1), the pore sizes were smaller for higher temperatures. As we would go up in the membranes, the pore sizes were larger (Fig. 4.3 (a)). This would bring forth funnel shaped pores at higher temperatures. These two data sets also show that the top openings of all pores at various temperatures were within 10-15% of largest pore sizes achieved at 400 °C but the lower size, arguably the smallest constrictions of the pores varied considerable with temperature used for curing.

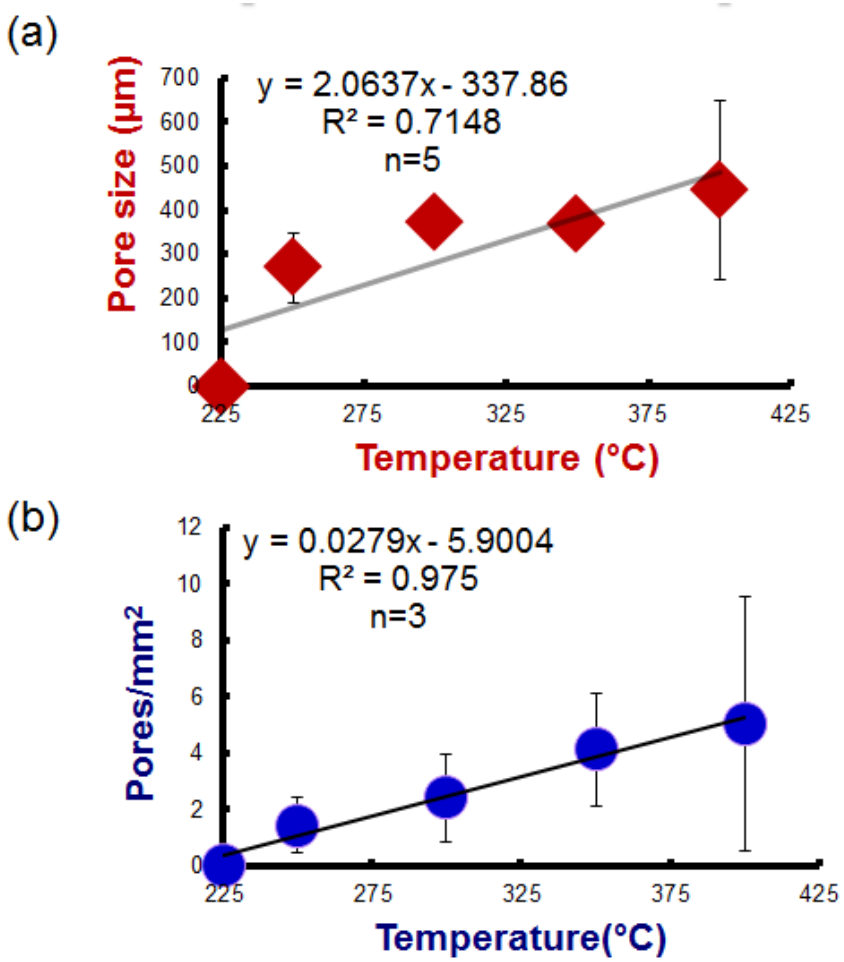

Figure 4.3 Effects of temperature on (a) Average pore size and (b) Porosity.

Figure 4.4 shows the distinct arrangements of microchannel resulting from the two different approaches undertaken to disperse PDMS pre-polymer. PEO polymers clustered to form micelles when these came in contact with PDMS. PU exhibited similar reactions. Micellar shapes are common because of hydrophilic/hydrophobic interactions [54, 55]. After melting PEO or PU, PDMS was gradually poured on the top of these hydrophilic molecules from one end to another. This kept hydrophilic particles intact in their original positions (Fig. 4.4 (a)). This phenomenon led to formation of microchannels that were in close vicinity localized in confined

area. However when PDMS was poured in a way that disturbed the original arrangement, channel formation was positioned in two ways. When hydrophilic particles were not completely molten, the solution moved as small stream and branched to form channels (Fig. 4.4 (c)). At times where the hydrophilic particles were completely molten and spread in a large area, the channels were generated along the line where hydrophilic and hydrophobic molecules interfaced each other (Fig. 4.4 (d) and (e)).

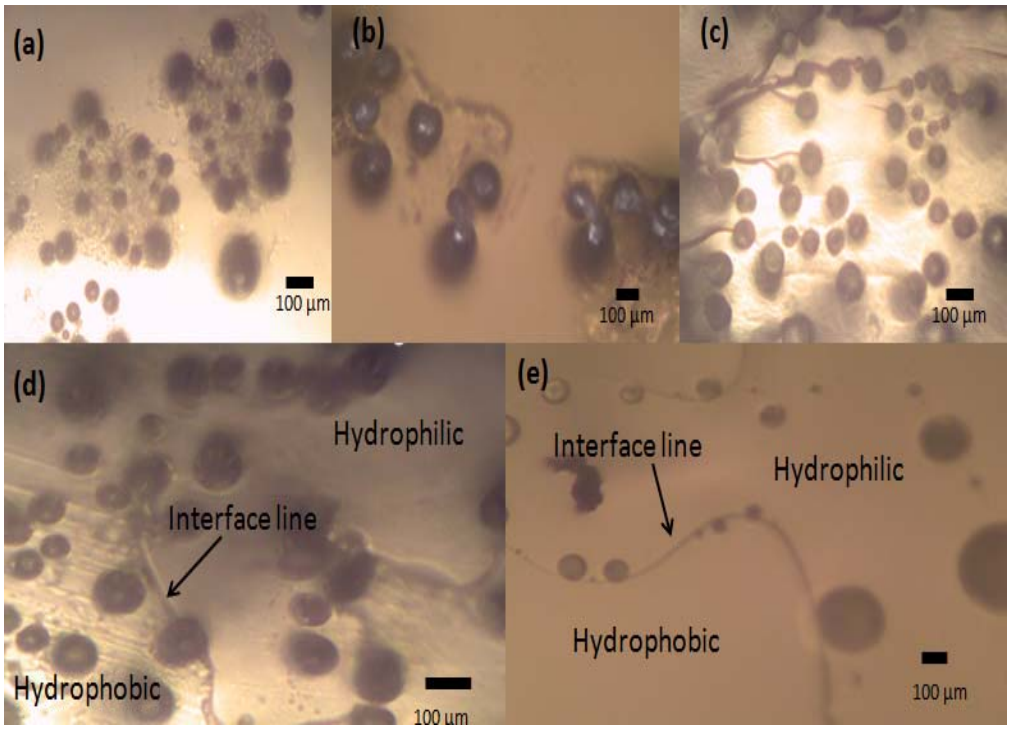

Figure 4.4 Microchannel arrangements at hydrophilic/hydrophobic interface. (a) PDMS is placed gradually without disintegrating initial position of PEO particles. (b) PDMS is placed gradually without disintegrating initial position of PU particles (c) When hydrophilic particles are not molten completely these form thin dendrite like branches forming into channels. (d) Channel formations at the interface line when PEO melts completely and (e) Channel formations at the interface line when PU particles melt completely.

When PDMS was continuously poured at just one point, the viscous hydrophilic polymer was pushed outwardly forming concentric rings. This was a result of phase separation when the

two repulsive molecules, hydrophilic molten and hydrophobic matrices of PDMS, came in contact. Stability of a mixture is favored by entropy and thermal fluctuation. When the mixtures have repulsive forces toward each other, molecules favor the separation of the two molecular species into two distinct macroscopic phases [8]. In the phase separation section of chapter three it was described that phase separation due to hydrophilic/hydrophobic interface occurred in different way (e.g. nucleation and spinodal decomposition). When PDMS was continuously poured on the molten, hydrophilic and viscous polymers, channels were separated by spinodal decomposition. Spinodal decomposition generally formed unstable biocontinous channels. However, in these experiments, the channels were stable because of PDMS polymerization. Due to the way the PDMS was poured, the hydrophilic molten clusters were phase separated in unique ways. When PDMS polymerized, several horizontal, continuous and concentric rings were formed at almost equal difference in diameters. (Fig. 4.5 (a)) This method also formed channels that were farther away from each other since particles pushed along the growing rings. Some of these rings were closed hollow channels while some were open (Fig. 4.5 (b) and 6(c)).

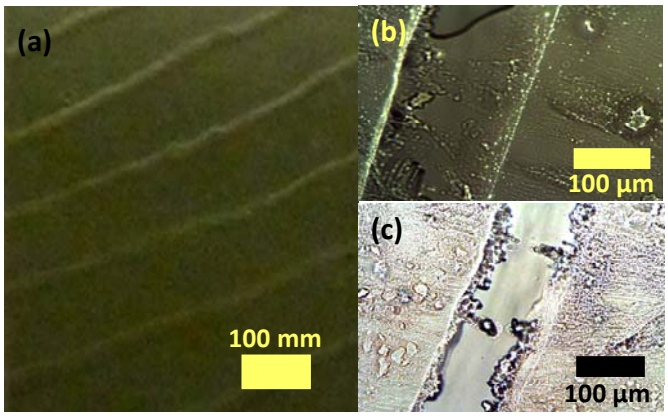

Figure 4.5 (a) Horizontal rings of hollow space formed during contact of PDMS with molten PEO. (b) and (c) Magnified views of single closed/opened hollow space formed, respectively.

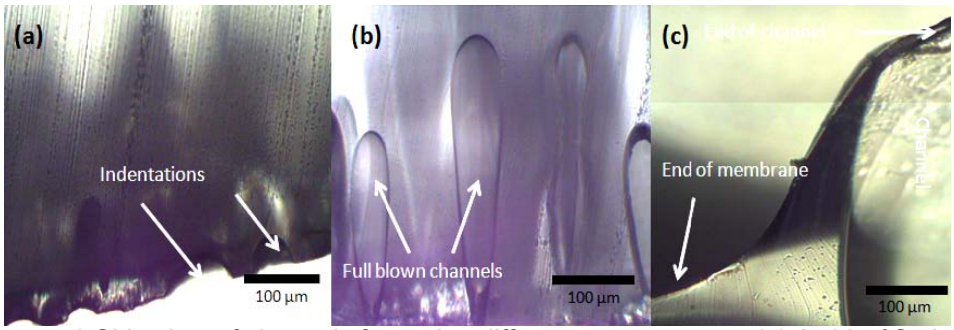

Figure 4.6 Side view of channels formed at different temperatures. (a) At 225 °C, there are only dent like formations. (b) Formation of microchannels at 250 °C. (c) Channel stretched out above the top of the membrane at 325 °C.

4.3.4 Characterization of Channel Lengths

Temperature showed a strong effect on the final outcome of channel length. Hydrophilic materials were more mobile when PDMS was in its viscous form. When the system was exposed to heat, entropy of these particles increased and these started to move upward while entropy of PDMS decreased due to formation of cross-linked gel like structure. There was no channel formation when temperature was less than 200 °C. At 225 °C, there were few round dent like structures (Fig. 4.6 (a)). At temperatures above 250 °C full blown channels appeared. The channels were larger at higher temperatures (Fig. 4.6 (c)). A monotonically proportional relationship between channel length and temperature is shown in figure 4.7. At lower temperatures, channel formation was slower compared to the rate of polymerization. Once cross-linking was completed and PMDS polymerized, formation of channels stopped leading to short channel formation. When the curing temperature used went from 250 °C to 325 °C, the channel lengths increased dramatically from 600 µm to 2274 µm. At high temperatures channel formation was slightly faster than PDMS polymerization therefore long channels were produced. If polymerization of PDMS was delayed channels would have been closed as seen for some iron-oxide particles in chapter 3. There it was shown that that when removal rate of iron-oxide is faster than rate of polymerization, there was no channel formation.

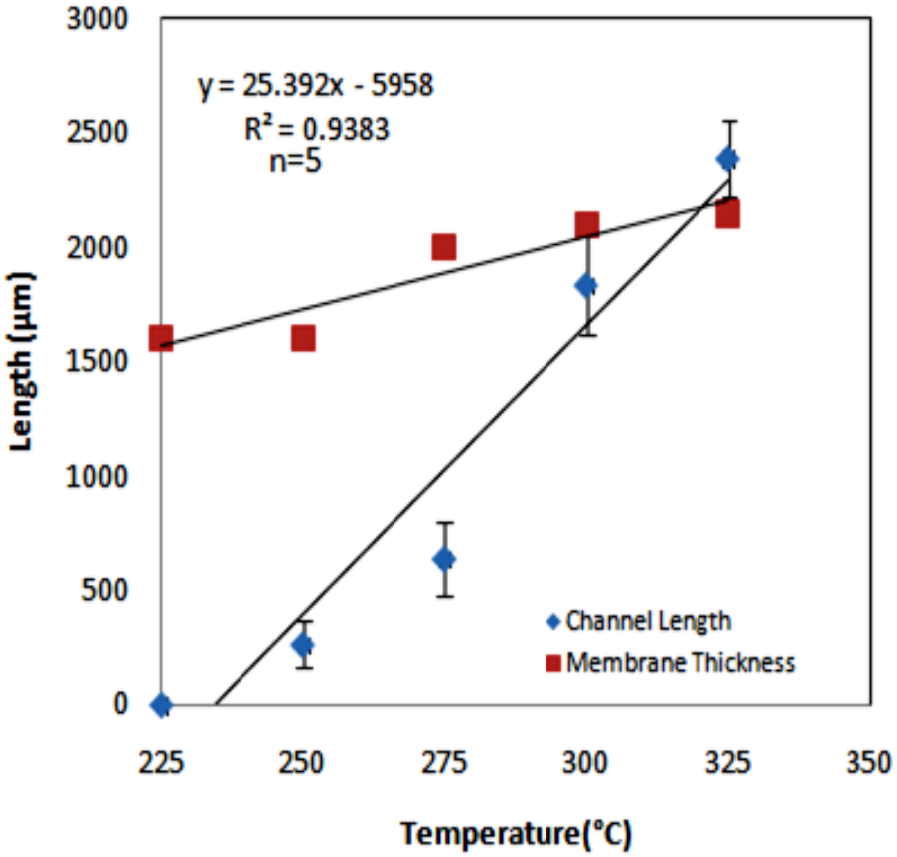

Figure 4.7 Channel length vs. temperature. Increasing temperature increases length of channels.

An interesting phenomenon was observed at 325 °C where the channel length surpassed the thickness of the membrane. At this temperature, the energy of hydrophilic particles gained from the temperature was enormous enough that some channels stretched above the top of the membrane (Fig. 4.6(c)). Increasing temperature above 325 °C, led to more channels surpassing the above surface of membrane. The reason these channels were above the top of the membrane instead of penetrating through was due to PDMS elasticity.

4.3.5 Capillary Action Driven Fluid Flow

Capillary effect-driven fluid flow experiments showed the integrity of microchannels and micromixing capability in these channels. Micromixing of solution was done without applying any

external forces. Capillary force (F_C) transferred fluid inside microchannel based on the diameter of channels (D), surface tension (σ), and contact angle (θ), as given below :[56]

$$F_C = \sigma \cos\theta \pi D \quad (4.1)$$

Plasma treated microchannels with diameter of 250 μm, and cut open from both ends, were exposed to red ink and blue ink from two sides. Fig. 4.8 (a) shows a strong capillary force pulling the fluid into the microchannels even when the channel inlet was not in direct contact with the fluid. Figure 4.8 (b) shows results for the solutions that were placed at opposite ends of the channels inlets. The two solutions migrated from one side to another, toward each other. Fusion of these two solutions was evident at the middle of the channel. This could provide potential device for controlled microchannel reactor for microfluidic system. Figure 4.8 (c) demonstrates the two fluid flowing using one inlet. The advantages of using this system was that the microchannel fabricated were capable of capillary action and PDMS being permeable to gases showed no trapped air between the two solutions (Fig. 4.8 (c)). This could have important implications in well-based immunoassays and simultaneous detection which is difficult to perform in traditional well plate system.

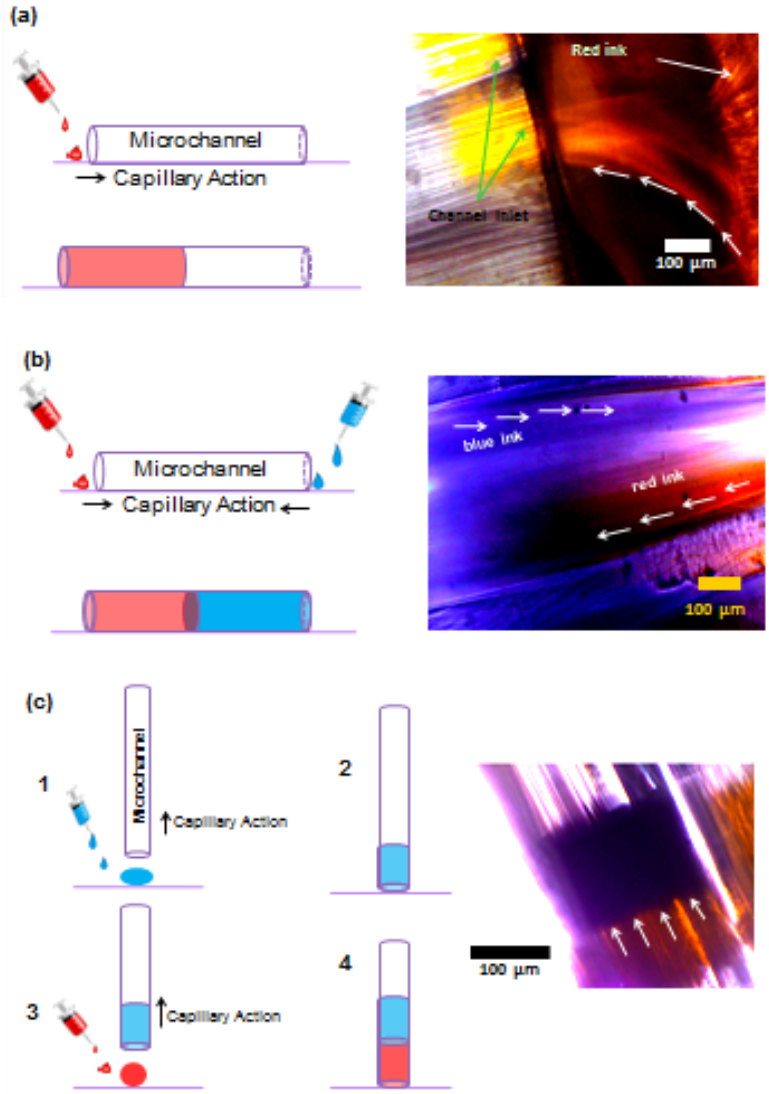

Figure 4.8 (a) Capillary force pulling fluid into the channels. The arrows inside the optical images show the direction of fluid flow. (b) Mixing of red and blue fluids by using capillary force from opposite inlets. (c) Red and blue ink flowing through same inlet.

Optical microscope data was used to measure distance of fluid traveled over time which enabled us to find velocity of fluid flow inside the channels (Fig. 4.9). The set of figure 4.9 shows optical images of fluid flow inside microchannel with respect to time. Distance of the flow was measured along the channel axis.

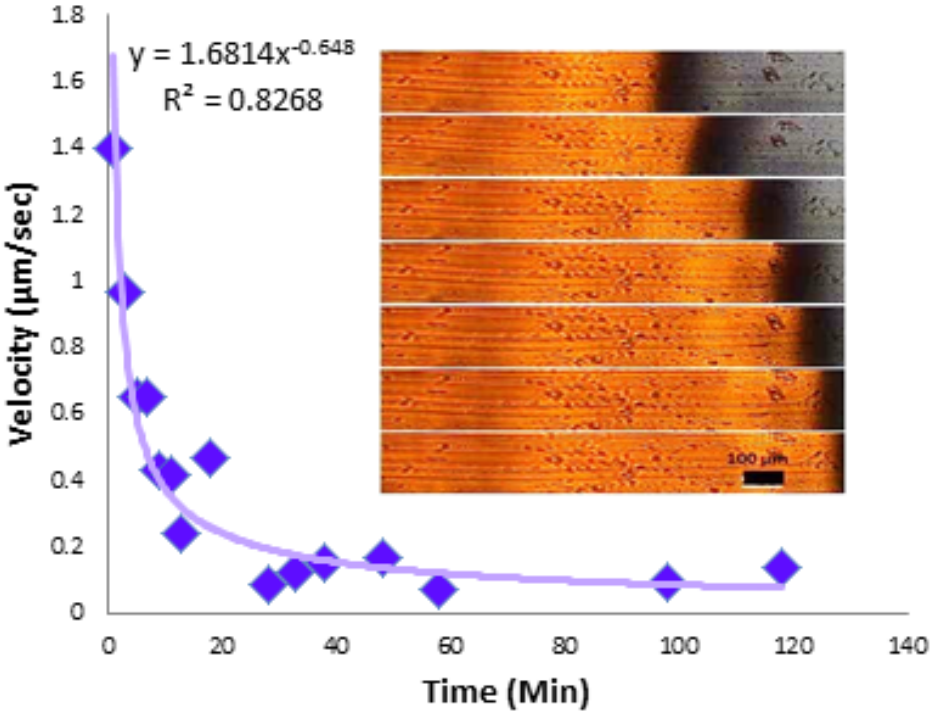

Figure 4.9 The flow of fluid inside microchannels. Plot shows decrease in fluid flow velocity with time. Inset shows time lapse images of red ink moving under capillary force.

Velocity was seen to be non-uniform through entire channel length. Velocity was high at the onset and started to decrease with distance and stabilized after certain time. Previously, it has been was reported that average velocity decreased toward center of the channel [57]. When fluid flowed from wide area to a narrow constricted area, velocity should have increased in order to maintain a constant flow rate but was seen to decrease [58]. There are surface charges on PDMS that may have contributed to counter-intuitive observations. Velocity (*V)* was calculated using Lagrangain description which states motion of a differential fluid volume using fixed reference frame. Velocity was measured as rate of change of position of fluid (*d*x) with respect to time (*dt*):

$$\boldsymbol{V} = \frac{\boldsymbol{dx}}{\boldsymbol{dt}} \qquad (4.2)$$

At the entrance of the microchannels, the initial velocity was 6.25 μm/s. For the first two minute the velocity was maintained but then it dropped gradually. It went down to 1.4 μm/s and all the way down to 0.085 μm/s in 30 minutes.

4.4 Conclusion

A self-assembled approach to synthesize circular microchannels ranging from few micrometer to hundreds of micrometers is demonstrated by using a simple interplay of hydrophilic and hydrophobic polymers. This chapter particularly dealt with channels driven by polymeric hydrophilic particles. Channels were characterized for chemical composition, size of channels, porosity and fluid flow. FTIR results showed that PEO traces were not detected in the porous PDMS membrane. Therefore the original properties of PDMS such as elasticity and transparency were maintained. Hydrophilic particles of PEO generated smaller pores compared to PU beads. Pore size and porosity were mainly controlled using temperature. The number of pores increased linearly with increasing temperature for all hydrophilic particles used in this thesis. Channel distributions could be controlled by controlling the pouring of PDMS. Channels in close vicinity were generated when PDMS was poured without disturbing the particles. But when PDMS was poured at one position, it spread in a circular motion dislocating the original position of hydrophilic particles along the way. This generated channels that were distributed farther apart. This also resulted in concentric circular distribution of PEO at almost equal distances apart. Various channel lengths were fabricated by controlling the thickness of the membrane and temperature. Fluid flow inside the channels was also characterized by measuring velocity change over time. High velocity was recorded at the inlet of channels and it was followed by a major drop toward the center.

CHAPTER 5

FUTURE WORK

5.1 Controlled Alignment of Self-assembled Channels

During the fabrication of micro/nanochannels, a high degree of precision and uniformity is required to produce efficient functional devices. Highly organized micro/nanochannels are useful to run large samples simultaneously. These can be also important for many applications in biological sciences. The self-assembled channels focused in this thesis can be further explored for better alignment, controlled porosity and custom-designed fluid flow. An experiment was conducted to explore the alignment by replacing hotplate with concentrated source of heat. Heat supplied through microwire was able to align the self-assembled channels linearly along the wire (Fig. 5.1). The heat on the microwire was formed by passing 9 mA current. The voltage and temperature through the microwire was measured to be 34.56 V and 80°C, respectively. This technique formed channels that were only aligned along the microwire. By further exploring this technique, it is possible to achieve well organized microwell devices.

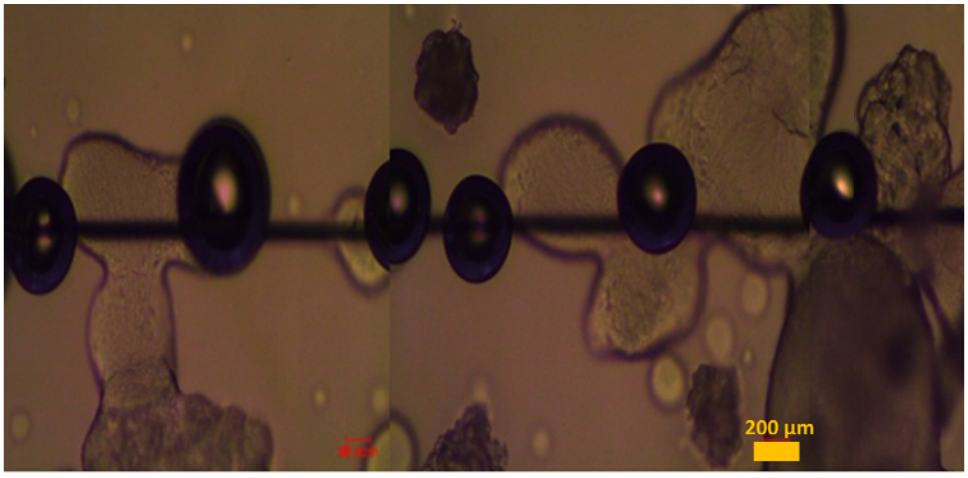

Figure 5.1 Alignment of microchannel using microwire for heat supply

5.2 Hydrogen Storage Container

This technique can also have important applications in the field of hydrogen storage. Hydrogen is one of the important sources of clean energy. It has highest energy content by weight however lowest energy by volume [59]. Thus challenges are encountered to develop an effective way to store this energy. Even though researchers have found ways to store hydrogen using high pressure and temperature, the system is complicated and inefficient [60]. Metal hydride technique is one of alternative techniques proposed for hydrogen storage. Metal hydride embedded in a PDMS membrane can potentially serve as a way to store hydrogen. The motivation for this idea is based on the results found during iron-oxide nanoparticle experiments of chapter 3. Instead of iron-oxide nanoparticles different type of metals such as iron, lithium, or magnesium can be used effectively to absorb hydrogen molecules. The challenge with the metal hydride storage is that it is unstable. Here we propose a second storage method to keep the metal hydride stable. Metal hydride can be embedded inside while polymerizing the PDMS to secure the stability. This technique is shown in figure 5.2 where iron-oxide particles are embedded inside PDMS parallel to each other using magnetic field.

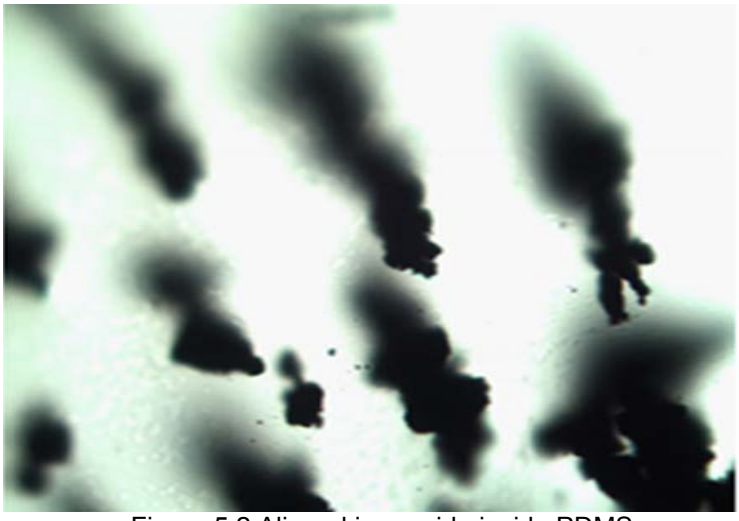

Figure 5.2 Aligned iron-oxide inside PDMS

Since PDMS is highly permeable to gases and also has elastic behavior, it could be an ideal material for such type of storage. Hydrogen can easily diffuse though the PDMS membrane and react with the metals embedded inside the membrane to form metal hydride. Most metal hydride bonds are reversible under certain temperature conditions based on the type of metal used. The optimum temperature can be applied to release hydrogen when needed. This PDMS storage can be light weight and inexpensive. In addition to that the system can also be more efficient since metals will be stored in microchannel in strained form as shown in figure 5.2, which maximizes interface of metals to hydrogen.

REFERENCES

1. Chin, C., *Fabrication of Metallic Nanoparticles Arrays.* The Journal of Young Investigators, 2007. 16(5).
2. Dyson, R.W., *specialty polymer*. 1987, chapman and hall: new york p. aldrich catalog No. Z22,414-6.
3. Goyal, S., *Nanoscale Approches for Biomolecules Separation and Detection*, in *Bioengineering*. 2009, University of Texas at Arlington: Arlington.
4. Kawamura, M., et al., *Nanowires and nanorings at the atomic level.* Physical review letters, 2003. 91(9): p. 96102.
5. Sahasrabudhe, K., *Nanochannel Fabrication Using Thermomechanical Deformation of Thermoplastic*, in *Mechanical Engineering*. 2006, University of Maryland: Maryland. p. 101.
6. Cheng, Y., K. Sugioka, and K. Midorikawa, *Microfabrication of 3D hollow structures embedded in glass by femtosecond laser for Lab-on-a-chip applications.* Applied surface science, 2005. 248(1-4): p. 172-176.
7. Jeyantt S. Sankaran, S.G., Wintana T. Kahsai, Uyen H. T. Pham, and Samir M. Iqbal, *Self-Assembled Hydrophilic Interfaceing for Thermal Micro Assembly of Polymer (HITMAP).* American scientif publishers, 2011. 4(3): p. 1-6.
8. Prum, R.O., et al., *Development of colour-producing -keratin nanostructures in avian feather barbs.* Journal of The Royal Society Interface, 2009. 6(Suppl 2): p. S253.
9. Perry, J.L. and S.G. Kandlikar, *Review of fabrication of nanochannels for single phase liquid flow.* Microfluidics and Nanofluidics, 2006. 2(3): p. 185-193.
10. Hungbin Yu, Z.G., Chau fook Siong, Wang Shouhua, and Lee Feiwen, *Novel polydimethylsiloxane (PDMS) next term based microchannel fabrication method for previous termlab-on-a-chipnext term application.* ScineceDirect 2009. 137(2): p. 754-61.
11. Tan, W., et al., *Miniaturized capillary isoelectric focusing in plastic microfluidic devices.* Electrophoresis, 2002. 23(20): p. 3638-3645.
12. Mitchell, P., 2001.
13. Meldrum, D.R. and M.R. Holl, *Microscale bioanalytical systems.* Science, 2002. 297(5584): p. 1197.
14. Herr, A.E., et al., *On-chip coupling of isoelectric focusing and free solution electrophoresis for multidimensional separations.* Analytical chemistry, 2003. 75(5): p. 1180-1187.
15. Harrison, D.J., et al., *Micromachining a miniaturized capillary electrophoresis-based chemical analysis system on a chip.* Science, 1993. 261(5123): p. 895.
16. Burns, M.A., *Everyone's a (future) chemist.* Science, 2002. 296(5574): p. 1818.
17. Williams, V., et al., *Microfluidic enabling platform for cell-based assays.* Journal of the Association for Laboratory Automation, 2002. 7(6): p. 135-141.
18. McDonald, J.C., et al., *Fabrication of microfluidic systems in poly (dimethylsiloxane).* Electrophoresis, 2000. 21(1): p. 27-40.
19. Branham, M.L., et al., *Rapid prototyping of micropatterned substrates using conventional laser printers.* Journal of materials research, 2002. 17(7): p. 1559-1562.

20. Makamba, H., et al., *Surface modification of poly (dimethylsiloxane) microchannels.* Electrophoresis, 2003. 24(21): p. 3607-3619.
21. Fidkowski, C., et al., *Endothelialized microvasculature based on a biodegradable elastomer.* Tissue engineering, 2005. 11(1-2): p. 302-309.
22. Liu, R.H., et al., *Passive mixing in a three-dimensional serpentine microchannel.* Microelectromechanical Systems, Journal of, 2000. 9(2): p. 190-197.
23. Wu, H., et al., *Fabrication of complex three-dimensional microchannel systems in PDMS.* Journal of the American Chemical Society, 2003. 125(2): p. 554-559.
24. Tolfree, D.W.L., *Microfabrication using synchrotron radiation.* Reports on Progress in Physics, 1998. 61: p. 313.
25. McDonald, J.C., et al., *Prototyping of microfluidic devices in poly (dimethylsiloxane) using solid-object printing.* Analytical chemistry, 2002. 74(7): p. 1537-1545.
26. Masuda, S., M. Washizu, and T. Nanba, *Novel method of cell fusion in field constriction area in fluid integration circuit.* Industry Applications, IEEE Transactions on, 1989. 25(4): p. 732-737.
27. Liu, A., et al., *Rapid method for design and fabrication of passive micromixers in microfluidic devices using a direct-printing process.* Lab Chip, 2005. 5(9): p. 974-978.
28. Fujii, K.H.M. and I. Endo. *HYDROPHOBIC MICROCAPILLARY VENT FOR PNEUMATIC MANIPULAITON OF LIQUID IN uTAS*. 1998: Kluwer Academic Publishers.
29. DeBusschere, B.D., D.A. Borkholder, and G.T.A. Kovacs. *Design of an integrated silicon-PDMS cell cartridge*. 1998.
30. Campbell, C.J., et al., *One-step multilevel microfabrication by reaction-diffusion.* Langmuir, 2005. 21(1): p. 418-423.
31. Schneega, I., R. Brautigam, and J.M. Kohler, *Miniaturized flow-through PCR with different template types in a silicon chip thermocycler.* Lab on a Chip, 2001. 1(1): p. 42-49.
32. Kikutani, Y., et al., *Glass microchip with three-dimensional microchannel network for 2× 2 parallel synthesis.* Lab on a Chip, 2002. 2(4): p. 188-192.
33. Lee, G.B., et al., *The hydrodynamic focusing effect inside rectangular microchannels.* Journal of Micromechanics and Microengineering, 2006. 16: p. 1024.
34. Koesdjojo, M.T., et al., *Two-stage polymer embossing of co-planar microfluidic features for microfluidic devices.* Sensors and Actuators B: Chemical, 2008. 131(2): p. 692-697.
35. Fuerstman, M.J., et al., *The pressure drop along rectangular microchannels containing bubbles.* Lab on a Chip, 2007. 7(11): p. 1479-1489.
36. Mijatovic, D., J.C.T. Eijkel, and A. Van Den Berg, *Technologies for nanofluidic systems: top-down vs. bottom-up—a review.* Lab on a Chip, 2005. 5(5): p. 492-500.
37. Hoeben, F.J.M., et al., *About supramolecular assemblies of -conjugated systems.* Chemical reviews, 2005. 105(4): p. 1491-1546.
38. Muthukumar, M., C.K. Ober, and E.L. Thomas, *Competing interactions and levels of ordering in self-organizing polymeric materials.* Science, 1997. 277(5330): p. 1225.
39. Valkama, S., et al., *Self-Assembled Structures in Diblock Copolymers with Hydrogen-Bonded Amphiphilic Plasticizing Compounds.* Nat. Mater, 2004. 3: p. 872.
40. Bottari, G., et al., *Phthalocyanine- Carbon Nanostructure Materials Assembled through Supramolecular Interactions.* The Journal of Physical Chemistry Letters. 2: p. 905-913.
41. Venumadhav, K. and et al., *Entropy driven spontaneous formation of highly porous films from polymerâ€“nanoparticle composites.* Nanotechnology, 2009. 20(42): p. 425602.

42. LÃ¶tters, J.C., et al., *The mechanical properties of the rubber elastic polymer polydimethylsiloxane for sensor applications.* Journal of Micromechanics and Microengineering, 1997. 7: p. 145.
43. Mata, A., A.J. Fleischman, and S. Roy, *Characterization of polydimethylsiloxane (PDMS) properties for biomedical micro/nanosystems.* Biomedical microdevices, 2005. 7(4): p. 281-293.
44. Espino, B., *Phase Separation of a Binary Mixture*, in *Department of physics* 2006, Kansas State University: Kansas.
45. Krishnan, R.S., et al., *Self-assembled multilayers of nanocomponents.* Nano letters, 2007. 7(2): p. 484-489.
46. Yethiraj, A., *Entropic and enthalpic surface segregation from blends of branched and linear polymers.* Physical review letters, 1995. 74(11): p. 2018-2021.
47. Zilman, A., et al., *Entropic phase separation in polymer-microemulsion networks.* Physical review letters, 2003. 91(1): p. 15901.
48. Flory, P.J. and W.R. Krigbaum, *Thermodynamics of high polymer solutions.* Annual review of physical chemistry, 1951. 2(1): p. 383-402.
49. Paul, J.F. and John Rehner, Jr., *Statistical Mechanics of Cross-Linked Polymer Networks II. Swelling.* The Journal of Chemical Physics, 1943. 11(11): p. 521-526.
50. Krishnamoorti, R., R.A. Vaia, and E.P. Giannelis, *Structure and dynamics of polymer-layered silicate nanocomposites.* Chemistry of Materials, 1996. 8(8): p. 1728-1734.
51. Armstrong, J. and K. Hollyman, *General, Organic, and Biochemistry: An Applied Approach*: Brooks/Cole Pub Co.
52. Maex, K., et al., *Low dielectric constant materials for microelectronics.* Journal of Applied Physics, 2003. 93: p. 8793.
53. Yuan, J., et al., *The "crew-cut" aggregates of polystyrene-b-poly (ethylene oxide)-b-polystyrene triblock copolymers in aqueous media.* European polymer journal, 2003. 39(4): p. 767-776.
54. Alexandridis, P., J.F. Holzwarth, and T.A. Hatton, *Micellization of poly (ethylene oxide)-poly (propylene oxide)-poly (ethylene oxide) triblock copolymers in aqueous solutions: thermodynamics of copolymer association.* Macromolecules, 1994. 27(9): p. 2414-2425.
55. Brown, W., et al., *Micelle and gel formation in a poly (ethylene oxide)/poly (propylene oxide)/poly (ethylene oxide) triblock copolymer in water solution: dynamic and static light scattering and oscillatory shear measurements.* The Journal of Physical Chemistry, 1991. 95(4): p. 1850-1858.
56. Ichikawa, N., K. Hosokawa, and R. Maeda, *Interface motion of capillary-driven flow in rectangular microchannel.* Journal of colloid and interface science, 2004. 280(1): p. 155-164.
57. Law, R.D., *Channel flow, ductile extrusion and exhumation in continental collision zones*. 2006: Geological Society Pub House.
58. F. Y. George A. Truskey, D.F.K., *Transport Phenomena in Biological System*. 2004, Upper Saddle River: Pearson Prentice Hall. 54-55.
59. Kikukawa, S., H. Mitsuhashi, and A. Miyake, *Risk assessment for liquid hydrogen fueling stations.* International Journal of Hydrogen Energy, 2009. 34(2): p. 1135-1141.
60. Ananthachar, V. and J.J. Duffy, *Efficiencies of hydrogen storage systems onboard fuel cell vehicles.* Solar Energy, 2005. 78(5): p. 687-694.

BIOGRAPHICAL INFORMATION

Wintana Kahsai was born in Ethiopia and moved to the United Sates in 2002 before completing high school. She continued her education and graduated from Arlington High School in Arlington, Texas. She pursued her higher education at Tarrant Community College and graduated in an associate degree with a Highest Academy Achievement and was named to the Dean's List. During her stay, she was recipient of the Computer Science, Engineering, and Mathematics Scholarship (CSEMS).

In 2007, she transferred to the University of Texas at Arlington and joined the department of Biomedical Engineering for dual master's program. She had an opportunity to work in Nano-bio lab with Dr. Samir Iqbal in 2009. Her research work focused in fabrication of microfluidics which expanded her knowledge in biology, chemistry, physics and polymers. She presented her works in many conferences and involved herself through kids outreach programs in campus.